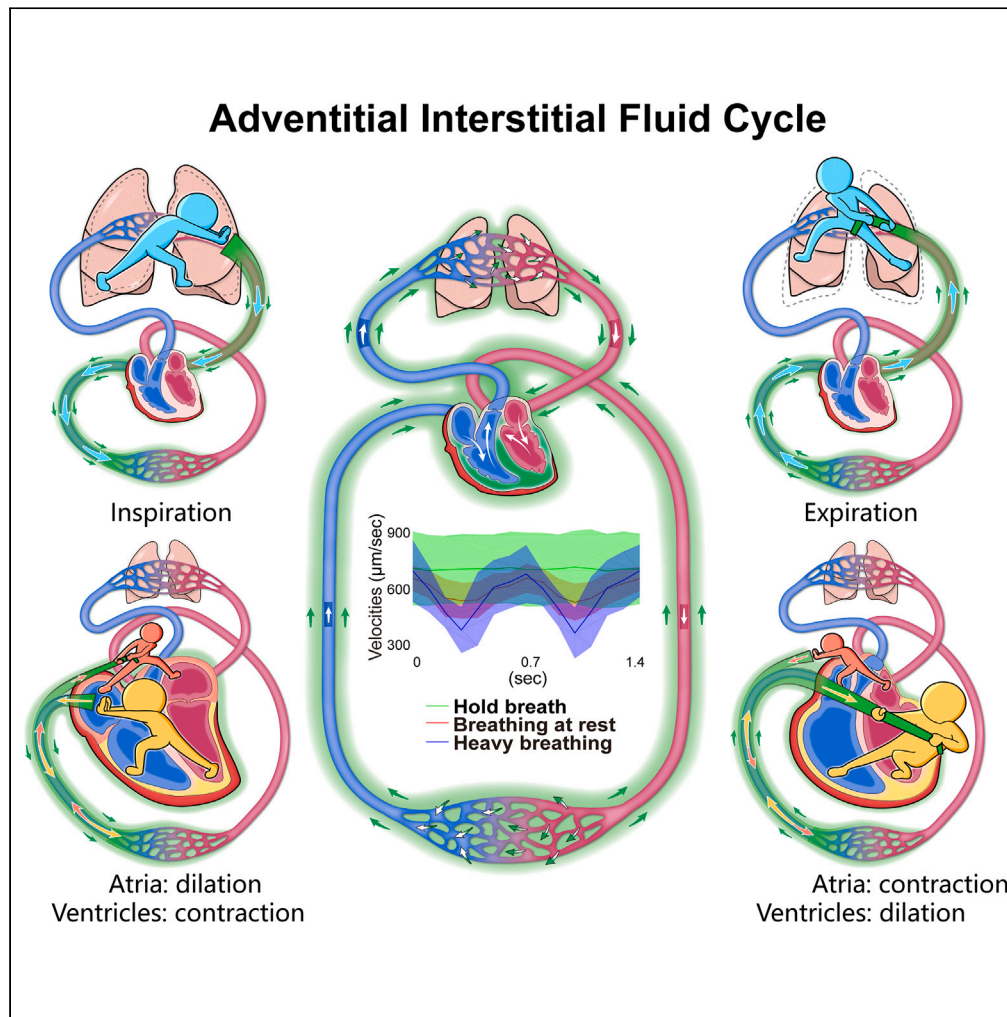


Article

# Regulation of interstitial fluid flow in adventitia along vasculature by heartbeat and respiration



Hongyi Li, Bei Li, Wenqi Luo, ..., Hua Li, Chao Ma, Fusui Ji

leehongyi@bjhmoh.cn (H.L.)  
 lihua@ict.ac.cn (H.L.)  
 machao@ibms.cams.cn (C.M.)  
 jifusui0367@bjhmoh.cn (F.J.)

**Highlights**

Synergistic actions of heart and lungs generate a to-and-fro flow of adventitial ISF

Heartbeat and respiration regulate adventitial ISF to flow along vasculature

ISF flows in “matrix-membranes channels” rather than a vascular conduit

Cardiovascular system can also transport and regulate ISF through the body



## Article

## Regulation of interstitial fluid flow in adventitia along vasculature by heartbeat and respiration

Hongyi Li,<sup>1,2,16,17,\*</sup> Bei Li,<sup>1,16</sup> Wenqi Luo,<sup>3,16</sup> Xi Qi,<sup>4</sup> You Hao,<sup>5</sup> Chaozhi Yang,<sup>6</sup> Wenqing Li,<sup>1</sup> Jiazheng Li,<sup>7</sup> Zhen Hua,<sup>7</sup> Tan Guo,<sup>8</sup> Zhijian Zheng,<sup>9</sup> Xue Yu,<sup>10</sup> Lei Liu,<sup>11</sup> Jianping Zhao,<sup>10</sup> Tiantian Li,<sup>10</sup> Dahai Huang,<sup>2</sup> Jun Hu,<sup>12,13</sup> Zongmin Li,<sup>6</sup> Fang Wang,<sup>10</sup> Hua Li,<sup>5,\*</sup> Chao Ma,<sup>14,15,\*</sup> and Fusui Ji<sup>10,\*</sup>

## SUMMARY

**Converging studies showed interstitial fluid (ISF) adjacent to blood vessels flows in adventitia along vasculature into heart and lungs. We aim to reveal circulatory pathways and regulatory mechanism of such adventitial ISF flow in rat model. By MRI, real-time fluorescent imaging, micro-CT, and histological analysis, ISF was found to flow in adventitial matrix surrounded by fascia and along systemic vessels into heart, then flow into lungs via pulmonary arteries and back to heart via pulmonary veins, which was neither perivascular tissues nor blood or lymphatic vessels. Under physiological conditions, speckle-like adventitial ISF flow rate was positively correlated with heart rate, increased when holding breath, became pulsative during heavy breathing. During cardiac or respiratory cycle, each dilation or contraction of heart or lungs can generate to-and-fro adventitial ISF flow along femoral veins. Discovered regulatory mechanisms of adventitial ISF flow along vasculature by heart and lungs will revolutionize understanding of cardiovascular system.**

## INTRODUCTION

Since *William Harvey* discovered blood circulation in 1628, and the *Starling's hypothesis* was proposed in 1896, the motion of extracellular fluid throughout the body is believed to include a rapid circulation of blood and lymph, and a constant movement of the interstitial fluid (ISF) through extracellular matrix after filtrated from the capillary walls. To date, long-standing efforts have found that the ISF could not only diffuse around tissue cells but also flow along blood vessels or in the interstitial compartment of certain tissues or organs over a long distance, such as the perivascular spaces (PVS) in the brain, thymus, liver, and several other organs,<sup>1-9</sup> the interstitial tissue channels between capillaries and initial lymphatic vessels,<sup>10,11</sup> the interstitial spaces of tumors,<sup>12,13</sup> etc. These ISF flows are distributed regionally near the arterioles, capillaries

<sup>1</sup>Research Center for Interstitial Fluid Circulation, Beijing Hospital, National Center of Gerontology, Institute of Geriatric Medicine, Chinese Academy of Medical Sciences, Beijing 100730, P.R. China

<sup>2</sup>Department of Geriatrics, Beijing Hospital, National Center of Gerontology, Institute of Geriatric Medicine, Chinese Academy of Medical Sciences, Beijing 100730, P.R. China

<sup>3</sup>Department of Cardiac Surgery, Beijing Hospital, National Center of Gerontology, Institute of Geriatric Medicine, Chinese Academy of Medical Sciences, Beijing 100730, P.R. China

<sup>4</sup>Peking University Fifth School of Clinical Medicine, Beijing Hospital, National Center of Gerontology, Institute of Geriatric Medicine, Chinese Academy of Medical Sciences, Beijing 100730, P.R. China

<sup>5</sup>Institute of Computing Technology, Chinese Academy of Sciences, Beijing 100190, P.R. China

<sup>6</sup>School of Computer Science and Technology, China University of Petroleum (East China), Qingdao 266580, P.R. China

<sup>7</sup>Department of Anesthesiology, Beijing Hospital, National Center of Gerontology, Institute of Geriatric Medicine, Chinese Academy of Medical Sciences, Beijing 100730, P.R. China

<sup>8</sup>Department of Radiology, Beijing Hospital, National Center of Gerontology, Institute of Geriatric Medicine, Chinese Academy of Medical Sciences, Beijing 100730, P.R. China

<sup>9</sup>Department of Acupuncture, Beijing Hospital, National Center of Gerontology, Institute of Geriatric Medicine, Chinese Academy of Medical Sciences, Beijing 100730, P.R. China

<sup>10</sup>Department of Cardiology, Beijing Hospital, National Center of Gerontology, Institute of Geriatric Medicine, Chinese Academy of Medical Sciences, Beijing 100730, P.R. China

<sup>11</sup>Department of Pharmacy, Beijing Hospital, National Center of Gerontology, Institute of Geriatric Medicine, Chinese Academy of Medical Sciences, Beijing 100730, P.R. China

<sup>12</sup>Key Lab of Interfacial Physics and Technology, Shanghai Institute of Applied Physics, Chinese Academy of Sciences, Shanghai 201210, P.R. China

<sup>13</sup>Shanghai Synchrotron Radiation Facility, Shanghai Advanced Research Institute, Chinese Academy of Sciences, Shanghai 201210, P.R. China

<sup>14</sup>Institute of Basic Medical Sciences, Chinese Academy of Medical Sciences, Department of Human Anatomy, Histology and Embryology, School of Basic Medicine, Peking Union Medical College, Beijing 100005, P.R. China

<sup>15</sup>Chinese Institute for Brain Research, Beijing 100005, P.R. China

<sup>16</sup>These authors contributed equally

<sup>17</sup>Lead contact

\*Correspondence: leehongyi@bjhmoh.cn (H.L.), lihua@ict.ac.cn (H.L.), machao@ibms.cams.cn (C.M.), jifusui0367@bjhmoh.cn (F.J.)

<https://doi.org/10.1016/j.isci.2024.109407>



and venules at the ends of the vascular tree, and regulated by hydrostatic and osmotic pressure differences,<sup>14</sup> capillary filtration coefficient, pumping by lymphatic system,<sup>15</sup> shear stresses generated by blood flow in the vascular microenvironment like the hypothesis of perivascular pump,<sup>16,17</sup> and etc. In brain, the cerebrospinal fluid (CSF) and blood flow were found to be influenced by respiration and cardiac activity in human studies using MRI.<sup>18–21</sup> Recently, converging studies have shown that the ISF adjacent to arteries and veins can also flow in the adventitia along the vasculature into the heart and lungs under an unknown regulatory mechanism.

In brain by intracisternal injection of ovalbumin-conjugated fluorescent tracer, the ISF flow was found in the PVS along the penetrating arteries, arterioles, capillaries, and venules as well as the large-caliber draining veins of mice.<sup>6,8</sup> In the body by interstitial injection of water-soluble low-molecular-weight fluorescent or paramagnetic tracers into perivascular tissues, our research group found that the ISF was illustrated by the tracers to flow longitudinally in the adventitial connective tissues along major arteries and veins from the extremities to the heart and lungs in animal models and human subjects.<sup>22–25</sup> In rabbits by the injection of the fluorescent tracer into the ankle hypodermis of rabbits, such adventitial ISF was visualized to flow along the saphenous and femoral veins, the inferior vena cava in the abdomen and thorax, and into the heart, while diffusing into the perivascular tissues along the way, and the capillaries, venules, and lymphatic vessels within them and back into blood circulation.<sup>22</sup> The calculated velocity of the continuous fluorescent adventitial ISF flow along the femoral veins was 3.6–15.6 mm/s.<sup>25</sup> By comparison, the velocities of the ISF flow in tumor tissues or connective tissues were 0.1–6.3  $\mu\text{m/s}$ .<sup>26–28</sup> In the pulmonary circulation of rabbits, the adventitial ISF was found to flow along the pulmonary vein from the lungs toward the heart.<sup>25,29</sup> The arterial adventitial ISF flow was demonstrated in the femoral artery of the rabbits, mice, and the posterior tibial artery of humans.<sup>22,23,25,30</sup> In the human cadaver experiments, the ISF from the thumb hypodermis could be “pulled” via the intact adventitial pathways along the superficial and deep veins of arm, axillary sheath, and superior vena cava into the atrial walls when the heart was repeatedly compressed by an automatic cardiac compressor.<sup>24</sup> Given arborescent vasculature exists everywhere throughout the body, elucidating the ISF flow along blood vessels will provide a novel mechanism for regulating the fluid environment in diverse tissues or organs by means of vascular vessels in humans and animals. On lights of the literatures and our previous explorations, we hypothesized that cardiac and respiratory movements are capable to regulate adventitial ISF flow through tunica adventitia along the systemic and pulmonary vasculature.

Tracking and accurately measuring such an *in vivo* adventitial ISF flow rate on micron to millimeter scale requires new methods. Using improved tracer imaging and quantitative speckle tracking techniques, we studied the whereabouts of the ISF flow along the adventitia of vascular vessels, the directions of the adventitial ISF flow along the blood vessels in the systemic and pulmonary circulation, and the mechanisms by which the heart and lungs regulate adventitial ISF flow in the rat. Moreover, to clarify the effects of each heartbeat or breath on the flow of adventitial ISF during cardiac or respiratory cycle, we performed experiments in dead rats by means of chest compressions, open-chest atrial or ventricular compressions, and mechanical ventilation, respectively.

## RESULTS

Our major findings are as follows briefly: (1) the adventitial ISF has found to flow in the adventitial matrix along the systemic and pulmonary vessels into the heart and lungs; (2) using quantitative speckle tracking velocimetry (STV), the adventitial ISF flow rate was found to be positively correlated with the heart rate (HR), increased when holding breath, and became pulsative during heavy breathing; (3) an empirical dynamic equation was proposed to illustrate the correlations of the adventitial ISF flow rate with the cyclical motions generated by the regular heartbeats and irregular respirations; (4) during respiratory cycle, it was observed that each expansion of the lungs during inflation generated a centrifugal flow of adventitial ISF along the femoral vein, while each contraction of the lungs during deflation generated a centripetal adventitial ISF flow; (5) during cardiac cycle, each dilation of atria or ventricles would generate a centripetal flow of adventitial ISF along the femoral vein, while each contraction of atria or ventricles generated a centrifugal adventitial ISF flow; (6) a working hypothesis of “matrix pump” was proposed to explain the driving mechanisms underlying the regulating of the adventitial ISF flow along the blood vessels by the movements of the heart and lungs; (7) the concentration of Esmolol in myocardium by adventitial infusion was found to be higher than that by intravenous injection starting from 3 min after administration.

### Visualized adventitial pathways originating from ankle dermis by Gd-DTPA and the differences from angiography

Consistent with our previous studies,<sup>22,25,30,31</sup> after administration of the water-soluble tracers into the perivascular tissues or adventitia of the large-caliber vascular vessels of lower limbs, it was found that the tracers would centripetally flow and visualize the arteries and veins starting from the administration point to the heart. When compared to angiography by intraluminal injection, it was the adventitial tissues distributed along the vessels were visualized by the adventitial infused tracers, rather than the blood within the lumen.

By MRI at 5 min after the hypodermic injection of the Gd-DTPA into the right ankle dermis, it was clearly found that the contrast enhanced the arterial and venous vessels of the right lower limb, but not the arteries and veins of the contralateral lower limb (Figure S1B, Video S1). In comparison, the intravascular contrast had visualized the arteries and veins of both right and left lower limbs at 5 min after the tail vein injection (Figure S1F, Video S2). At 10–20 min after the injection, the adventitial contrast gradually enhanced the arteries and veins of the contralateral lower limb, the aorta and IVC of the abdominal and thoracic cavities, kidney, and bladder, indicating that the adventitial contrast flowed along the vascular vessels and meanwhile entered the blood circulation (Figures S1C and S1D). At 40–50 min after the adventitial infusion or intravenous injection, the visualization of blood vessels began to weaken (Figures S1D and S1H). The results of dynamic MRI scanning suggested that the adventitial infused tracer enhanced the adventitial tissues along the blood vessels during about 5 min after the administration, and then gradually entered the blood circulation.

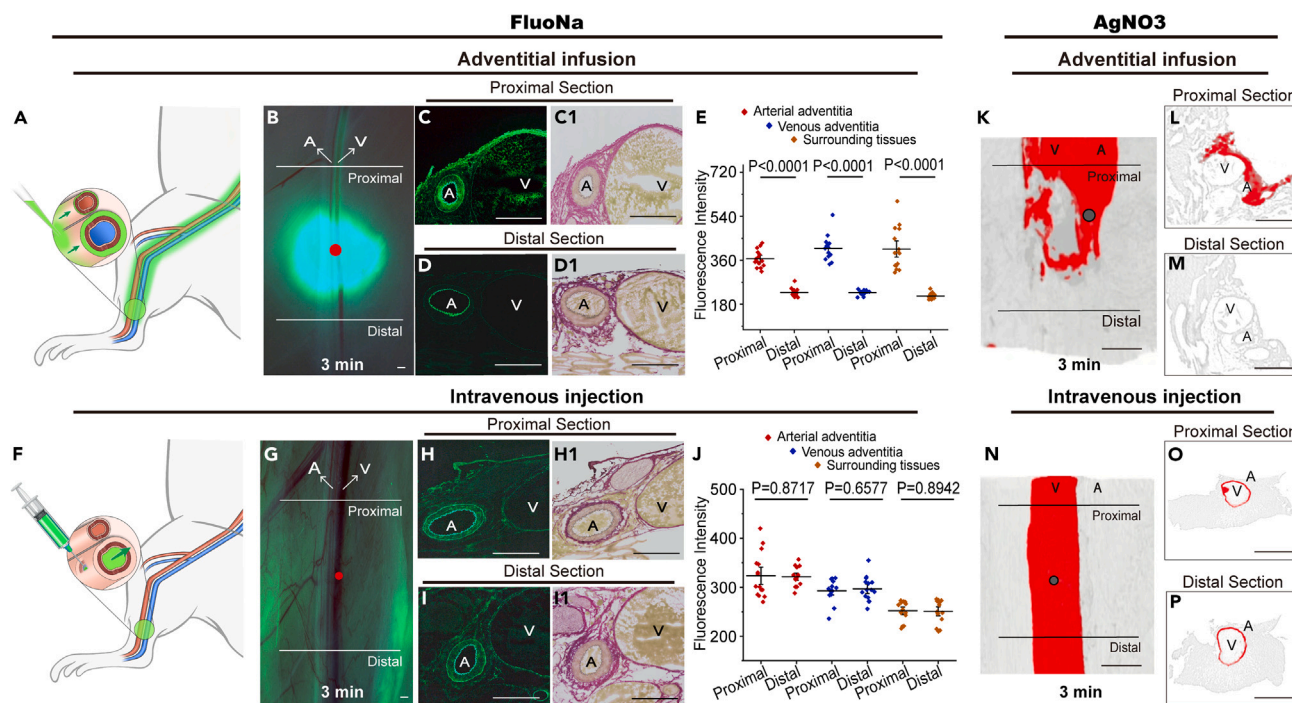


**Figure 1. Comparison of adventitial infusion and intravenous injection of the FluoNa and Silver nitrate in the lower limbs**

By fluorescence stereomicroscopy, (A and B) The FluoNa was infused into the adventitial pathways of the saphenous vessels, diffused around the infusion site (red point) and flowed centripetally along the vessels. Cross-sectional images showed the proximal (C and C1) but not the distal (D and D1) end of the adventitial pathways was stained by the FluoNa. The analysis of fluorescence intensity showed that the fluorescent signals of the arterial and venous adventitia, and the tissues surrounding the vessels in the proximal end were significantly stronger than those of distal end (E).

(F and G) The FluoNa was intravenously injected into the saphenous vein (red point). There were no significant differences of fluorescence intensity between the proximal (H and H1) and distal (I and I1) end of the adventitial pathways (J). Using SMCT, the adventitiously infused silver nitrate was found to flow along the proximal but not distal end of the adventitial pathways (K, L, and M). The intravenous silver nitrate enhanced the proximal and distal end of the vein together (N, O, and P). Scale bar: 500  $\mu$ m. The solid lines in (B, G, K, and N) indicated the sites of cross section at the proximal or distal end. A, artery. V, vein. In (E, and J), *t* test, mean  $\pm$  SEM, *n* = 3 rats.

### Visualized adventitial pathways originating from ankle dermis by real-time fluorescence stereomicroscopy, or SMCT and their differences from angiography

By real-time fluorescence stereomicroscopy or spectral micro-computed tomography (SMCT) at 3 min after the adventitial infusion, either the adventitial FluoNa or silver nitrate from the saphenous vessels was found to flow centripetally along the saphenous vessels (Figures 1B, 1K, 1G, and 1N; Video S12) and stained the proximal end (Figures 1C and 1L) but not the distal end (Figures 1D and 1M) of the vessels. By analyzing the real-time frozen sections, the fluorescence intensity of the proximal site was significantly stronger than those of the distal section in the adventitial infusion group (Figures 1C–1E). By comparison, there were no significant differences found between the proximal and distal ends in the angiography group (Figures 1H–1J). The SMCT results showed that the intravenous cavity of the saphenous vein was stained by the intravenously injected silver nitrate (Figures 1N–1P; Video S12).

### Cross-sectional of the intact or disrupted adventitial pathways of the femoral vessels that were stripped of perivascular tissues

To identify whether the location of adventitia ISF flow is in the perivascular tissues or adventitial matrix, we surgically striped of the perivascular tissues along a segment of femoral vessels and used real-time fluorescence stereomicroscopy to study the flow of the adventitial infused FluoNa (4 $\mu$ L, 0.1 g/L) in the adventitia of the isolated artery and vein. At 30 s after the adventitial infusion into the distal adventitial pathways on the saphenous vessels, the cross-sectional views showed that the FluoNa had stained the adventitia surrounding the isolated femoral artery and vein (Figures S2B and S2B1).

### Quantifying the longitudinal adventitial ISF flow along femoral artery and vein by fluorescent tracer

When the adventitia along the femoral vein and artery were disrupted by type I collagenase, it was found that the distal FluoNa cannot flow through and stain these femoral adventitial channels as well as the arterial wall (Figures 2D, 2D1, S2C, and S2C1). At the same time, the

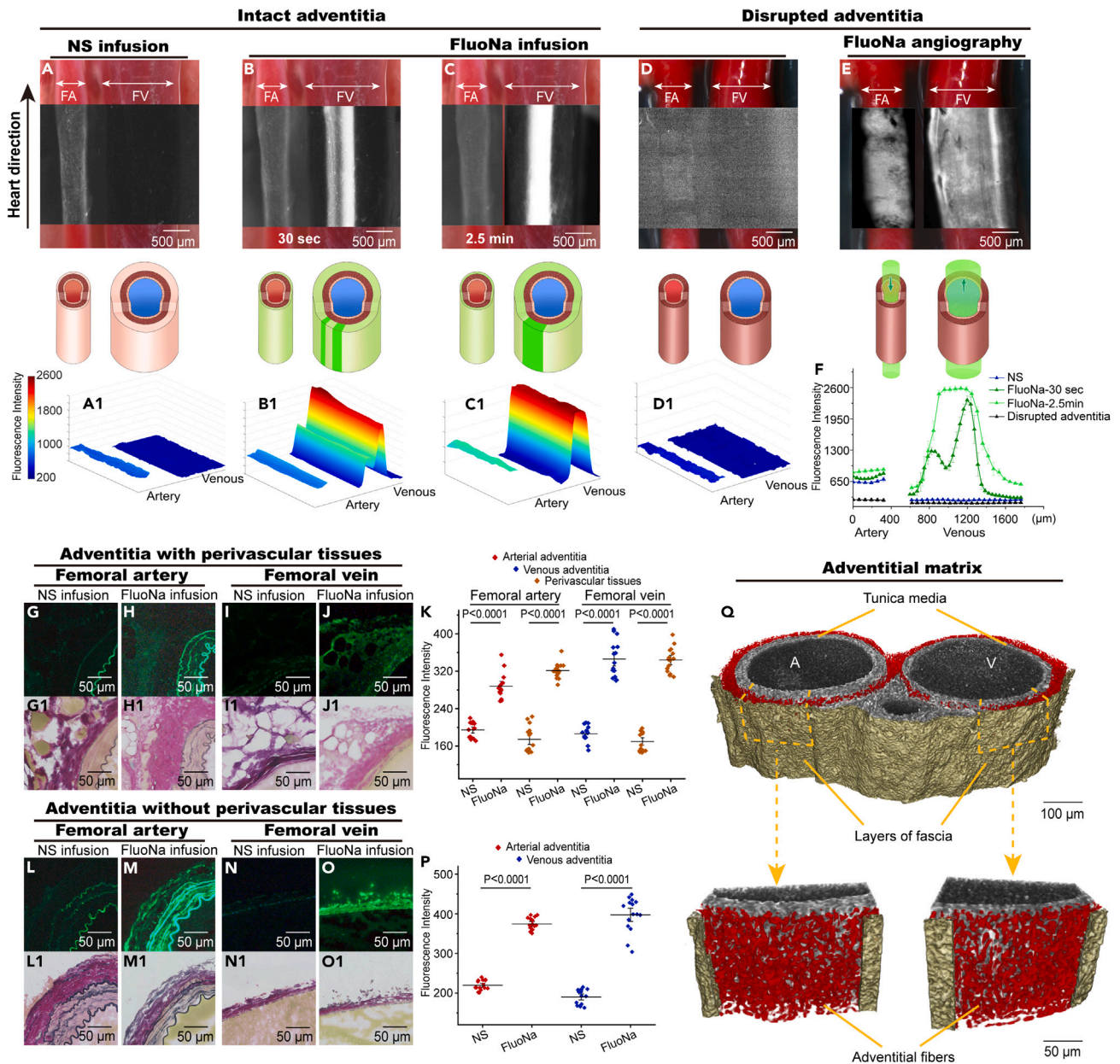


**Figure 2. Quantifying the longitudinal adventitial ISF flow along the femoral artery and vein that were stripped of perivascular tissues**

To clearly observe the longitudinal adventitial ISF flow, the femoral arteries and veins (A–E) were stripped of the perivascular connective tissues. Recorded by real-time fluorescence stereomicroscope, A, A1 showed that the fluorescence intensity of a femoral artery and vein was weaker by the adventitial infusion of NS. After the adventitial infusion of FluoNa into the distal adventitial pathways of the saphenous vessels, two linear fluorescent lines in the adventitial pathway were found along the side of the femoral vein at 30s (B) and converged into one wider fluorescent line channel at 2.5 min (C). When the adventitia of femoral vessels was disrupted by collagenase I (D), the distal FluoNa cannot flow through and stain the adventitial walls of the artery and vein. Meanwhile, the contralateral venous angiography confirmed that this femoral artery (D) was unobstructed, and the ipsilateral venous angiography showed this femoral vein (D) was also unobstructed (E). (A1, B1, C1, and D1) showed the intensity and distributions of the fluorescein along the arteries and veins detected by fluorescence stereomicroscopy. F showed that the changes in fluorescence intensity of the (A1, B1, C1, and D1). (G–J) were the cross-sectional views of femoral vessels by fluorescence microscopy and showed the results of the fluorescent adventitial ISF in the adventitia of femoral vessels having stained the perivascular tissues as well.

(G1–J1) were the bright field corresponding to (G–J).

(L–O) showed the results of the fluorescent ISF flowing in the adventitia of femoral vessels without the perivascular tissues.

(L1–O1) were the bright field corresponding to (L–O).

**Figure 2. Continued**

(H and H1) showed that the arterial adventitia, connective tissues surrounding the artery, and even the media were all stained by the FluoNa from the distal, and the fluorescence intensity was significantly stronger (K) than that of the control group G.

(J and J1) showed that the venous adventitia, connective tissues surrounding the vein, and even the media were all stained by the FluoNa from the distal, and the fluorescence intensity was significantly stronger (K) than that of the control group I.

(M and M1) showed that the arterial adventitia and media can be stained by the distal FluoNa even in the absence of perivascular tissues, and the fluorescence intensity was significantly stronger (P) than that of the control group L.

(O and O1) showed that the venous adventitia and media can be stained by the distal FluoNa in the absence of perivascular tissues, and the fluorescence intensity was significantly stronger (P) than that of the control group N.

(Q) The reconstructed three-dimensional views of the femoral artery and vein. The numbers of the adventitial fibers between the fascia and tunica media were calculated to be around 2504 (range from 2315 to 2796) along the femoral vein, and 2605 (range from 2450 to 2750) along the femoral artery. FA, femoral artery. FV, femoral vein. The arrows marking FA or FV refer to the inner diameter of the FA or FV under bright field. In (K and P), t test, mean  $\pm$  SEM, n = 3 rats.

angiography confirmed that both the femoral artery and vein were unobstructed (Figures 2E and Videos S3 and S4). Histological analysis of successive sections showed that the femoral artery and vein did not contain the vasa vasorum running continuously along the long axis of the vessels (Figures S3A–S3J). The lymphatic vessels were also present in the perivascular connective tissues but not within the adventitia of blood vessels (Figures S3K, S3K1, S3K2, and S3L). Thus, the tunica adventitia surrounded by fascia, rather than the conduit-like vasorum and lymphatics, were the histological structures for the longitudinal adventitial ISF flow. Estimated by micro-CT, the numbers of the adventitial fibers under its surrounding fascia were calculated to be around 2504 (range from 2315 to 2796) along the femoral vein, and 2605 (range from 2450 to 2750) along the femoral artery (Figure 2Q).

Following administration of the FluoNa by adventitial infusion onto the adventitia of distal vessels of the limbs under real-time stereomicroscopy with a high-resolution camera, two types of adventitial ISF flow were observed along the femoral vessels, early rapid flow, and subsequent speckle-like flow. Within 20 s after the start of the adventitial infusion, it was found that the FluoNa flowed rapidly along the femoral veins and formed two fluorescent lines along one side of the femoral vein. At subsequent 20–30 s when more FluoNa entered the adventitial pathways, the fluorescence intensity of these two fluorescent lines gradually increased (Figures 2B and 2B1), changed from thin to wide, and merged into a wider fluorescent line at about 120–150 s (Figures 2C, 2C1, S3A–S3D). Inside the wider fluorescent line along the femoral vein, the flow of the FluoNa was relatively stable and exhibited speckle-like between consecutive frames (Video S5). Limited by the current *in vivo* imaging technique, the longitudinal flow of fluorescent ISF in the femoral arterial adventitia was observed, but the speckle-like flow cannot be detected (Figures 2C, 2C1, and S3A).

In the relatively fixed HR and certain respiratory parameters, the flow rate measured in the adventitial pathways along the femoral veins was consistent when 1  $\mu$ L, 4  $\mu$ L, and 16  $\mu$ L of infusion fluid of the FluoNa were administrated into the distal end of the adventitial pathways (Table S1). Then one of infusion doses, 4  $\mu$ L was selected for per administration in the studies.

**The velocity of the rapid and speckle-like flow of adventitial ISF along the femoral vein**

Under physiological conditions with the HR of 290–460 bpm and certain respiratory parameters (RR: 90bpm, I/E: 1:2, TV: 4.0 mL), the rapid flow of the FluoNa along the femoral vein was recorded within 20 s after the administration and the calculated flow rate was 1.3–5.8 mm/s (Figure S4). At 2.5 min after administration, the continuous speckle-like flow was dynamically recorded along the femoral veins and the velocity was measured by STV (Figure S5A).<sup>32–35</sup> In the 10-min observation, we typically tracked around 130,000 speckles (Table S2). The median velocity of the calculated speckles was around 588.2  $\mu$ m/s (range 258.0–967.1  $\mu$ m/s), and the mean velocity was 598.1  $\pm$  107.7  $\mu$ m/s (Table S2). The velocity profile of the ISF flow field was uniform from the left edge to the right, from the bottom to the top (Figures S5B–S5E). By comparison with fluorescence angiography, the calculated velocity of the arterial blood flow was 188.5  $\pm$  57.6 mm/s, and the venous blood flow was 6.6  $\pm$  0.6 mm/s (n = 5 rats for each group).

The measured arterial and venous pressure were 98–112/80–88 mmHg, 5–9 mmHg under the HR of 360–430bpm (Table S3). By comparison, we found that only the FluoNa can exhibit the speckle-like flow along the adventitial pathways, while Rhodamine B and Indocyanine green cannot.

**Regulation of adventitial ISF flow along femoral vein by HR and respiration**

Using STV under physiological conditions, the flow rate of the adventitial ISF along the femoral vein was found to be associated with the HR and respiration. When the HR increased from 150 to 450 bpm, the flow rate of the adventitial ISF also increased (Figure 3B). When the apnea was present and the HR was 410–420 bpm, the median flow rate of the adventitial ISF was significantly faster than that of resting breathing (Figures 3C and 3C1). When breathing heavily with large amount of tidal volume (TV) (6.0 mL), a pulsatile flow of the adventitial ISF was displayed, the frequency of which was the same as the heavy breath (Figures 3C and 3C1).

When the HR of rats was 390–420 bpm, the frequency of the pulsed flow rate of the adventitial ISF was consistent with the respiratory rate (RR) (Figures 3D and 3D1); at different tidal volumes, the greater the TV, the greater the pulse amplitude of the adventitial ISF flow rate (Figures 3F and 3F1); I/E (1:1, 2:1, 1:2) determined the descending and ascending branches of the pulse (Figures 3H and 3H1).

When the heart of rats stopped beating and the lungs were ventilated repeatedly, the act of inflation can cause a centrifugal flow of the adventitial ISF, while the act of deflation induced a centripetal flow of the adventitial ISF. Correspondingly, the effects of the RR, TV, and the I/E ratio were consistent with those under physiological conditions (Figures 3E, 3E1, 3G, 3G1, 3I, and 3I1). Meanwhile, the measured venous pressures were significantly reduced to 0–1 mmHg by comparison with 5–7 mmHg under physiological conditions (Table S3).

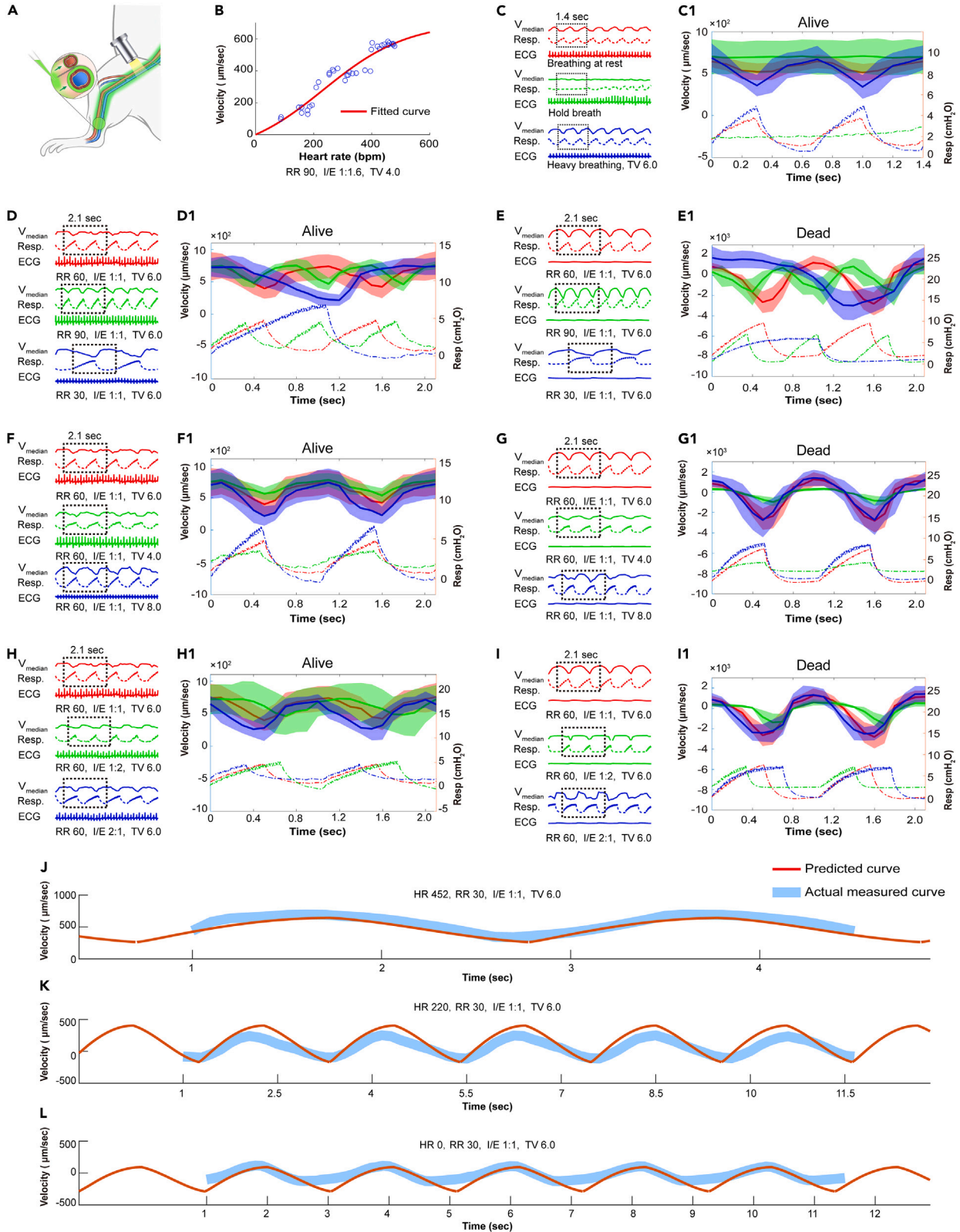


### Figure 3. Regulation of adventitial ISF flow in the venous adventitial pathways by HR and respiration

(A) Illustration of the observation on the adventitial ISF flow in the venous adventitial pathways of the femoral vessels.  
 (B) When the HR increased from 150 to 450 bpm, the flow rate of the adventitial ISF also increased (RR 90bpm, I/E 1:1, TV 4.0 mL, n = 1). The fitted curve was calculated based on sigmoid function.  
 (C and C1) When the breath held, like apnea, the adventitial ISF flow rate increased by comparison with that at resting breath. A heavy breath induced a pulsatile flow at the same frequency as the heavy breath.  
 (D, D1, E, and E1) The frequency of the pulsed flow was consistent with the RR in alive or dead rats.  
 (F, F1, G, and G1) The greater the tidal volume, the greater the pulse amplitude of adventitial ISF flow in alive or dead rats.  
 (H, H1, I, and I1) The inspiration and expiration (I/E) ratio (1:1, 2:1, 1:2) determined the descending and ascending branches of the pulse in alive or dead rats. In alive rats, the inflation can decelerate the centripetal adventitial ISF flow. In dead rats, the inflation can cause a centrifugal adventitial ISF flow, while the deflation induced a centripetal adventitial ISF flow. Each group of (C, D, E, F, G, H, and I) was sampled from 6 rats. The solid lines were the mean value and the shaded is the standard deviation of the median velocity of a total 6 rats in each group of (C1, D1, E1, F1, G1, H1, and I1), respectively. The dotted lines (Resp.) are the measured pressure on the surface of the body of a rat by the breathing band sensor, representing the changes of breathing.  
 (J) was from Video S6, (K) was Video S7, and (L) was Video S8. The HR of (J) was around 452bpm, (K) was 220bpm, and (L) was zero. The ventilation parameters of (J), (K), and (L) were all the same, the RR was 30 breaths/min, I/E was 1:1, and tidal volume was 6.0 mL. In either (J) or (K) or (L), the predicted curve (orange) calculated by this cyclical dynamic equation matched the actual measured curves (blue) of the adventitial ISF flow rate very well. Data were represented as mean ± SEM.

### The empirical dynamic equation for the regulation of adventitial ISF flow by heartbeat and respiration

Assuming that the adventitial pathway with diverse types of interior channels can be simplified as a cylindrical channel, and the ISF is an incompressible and Newtonian fluid with a low Reynolds coefficient, the general form of the correlation between the velocity ( $V_{max}$ ) and the pressure gradients ( $\Delta p$ ) over a given length of the channel will be

$$V_{max} = k * \Delta p \quad (\text{Equation 1})$$

$k$  is a continuous and determined by the properties of both fluid and adventitial pathways, such as the fluid's viscosity, length of the pathways, the radius of the point (at different positions in the channel) to the center of the channel (the Equation 6 in Note S1).

According to our experimental findings, there are two cyclical driving forces regulating the adventitial ISF flow along the femoral veins, the heartbeat and respiration.  $\Delta p_{heart}$  represents the driving forces generated by the regularly cyclical deformations of the heart and is related with the frequency  $\theta$  of the heartbeats.  $\Delta p_{lung}$  represents the driving forces generated by the irregularly cyclical deformations of the lungs and is related with the respirations, including the respiratory frequency  $F$ , TV  $V$ , inspiration-expiration ratio  $R$ . Therefore, we can get the empirical dynamic equation as

$$V_{max} = k * (\Delta p_{heart} + \Delta p_{lung}) = k * (F(\theta) + G(p_{lung})), \quad (\text{Equation 2})$$

where  $F$  and  $G$  are the functions related to the heartbeats and respirations, respectively. We can determine a function model depending on the observation and then derive the parameters of the function model via fitting method. The derivation process of the empirical equation was listed in the Note S1. The final equation of  $V_{max}$  will be

$$V_{max}(\theta, t, F, V, R, sp) = k * (\Delta p_{heart} + \Delta p_{lung}) = k * (F(\theta) + G(p_{measure})) = -139.6 + \frac{843.3}{1 + \exp\left(-4 * \log(3) * \frac{\theta - 234.1}{636}\right)} + \frac{800 * (V^2 + 2V)}{50 * 60 * F} * \left( \left| \sin\left(\frac{1}{60 * F * 3.3} * t - sp\right) \right| * \sqrt[3]{p_{measure}\left(\frac{1}{60 * F * 3.3} * t - sp, R\right)} - 600 \right), \quad (\text{Equation 3})$$

The parameter  $sp$  is referred to the starting phase ( $sp$ ) of the irregular cycle of the respiration and is determined individually by each case.  $t$  is referred to time. By comparison, the predicted curve (orange) calculated by this cyclical dynamic equation matched the actual measured curves (blue) of the adventitial ISF flow rate very well (Figures 3J–3L, Videos S6, S7, and S8).

Therefore, these revealed correlations between the adventitial ISF flow and the cyclical motions of heartbeat and respiration indicated that the ISF is able to pass through the interior channels (inter-channel) of the adventitial pathways in response to external forces. Considering the  $k$  represented the properties of a simplified cylindrical channel, we named the transport ability of the ISF flow through the diverse types of inter-channels of an adventitial pathway as hydraulic interfacial/inter-channel transportability (HIT, represented by  $T$ ). The empirical dynamic Equation 2 can be reformed as

$$V_{max} = T * (\Delta p_{heart} + \Delta p_{lung}) = T * (F(\theta) + G(p_{lung})) \quad (\text{Equation 4})$$

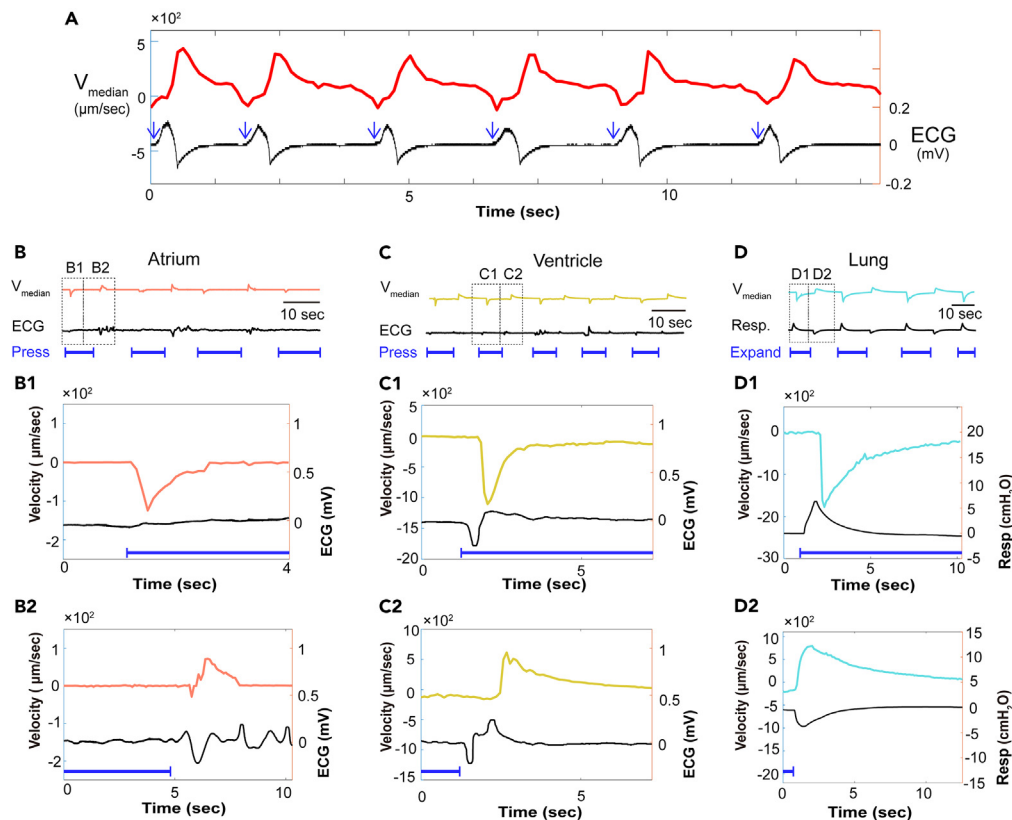


**Figure 4. To-and-fro motion of adventitial ISF in the femoral adventitial pathways during a cardiac and respiratory cycle**

(A) By repeated chest compressions at intervals of 2–3 s in the freshly dead rats, the contraction and dilation of the heart caused the same pulsatile flow of the adventitial ISF along the femoral veins. Blue arrow indicates the one-shot act of chest compression. When the chest cavity was opened, the atria or ventricles were continuously compressed for 10–15 s (blue line), and then released to allow the atria or ventricles to dilate on their own (B and C).

(B1 and C1) The compression of the atria or ventricles induced a centrifugal adventitial ISF flow.

(B2 and C2) The dilation of the atria or ventricles caused a centripetal adventitial ISF flow.

(D) The lungs were expanded by the 5 mL syringe for 10–15 s (blue line), and then contracted by the 5 mL syringe for another 10–15 s. D1 The expansion of the lungs induced a centrifugal adventitial ISF flow.

(D2) The contraction of the lungs caused a centripetal adventitial ISF flow.

$T$  is determined not only by  $k$  but also by the properties of the inter-channels of the adventitial pathways for fluid flow, such as the interfacial properties of the inter-channels of the adventitial pathways, the liquid content in the gel matrix, the connectivity of the fibrous scaffold of the adventitial matrix, temperature, pressure, etc. The HIT of diverse adventitial pathways needs further studies to be determined.

### To-and-fro motions of adventitial ISF along femoral vein during cardiac and respiratory cycle

By analyzing the changes of the mean velocity by STV, the effects of periodic deformations during the cardiac or respiratory cycle on the adventitial ISF flow along the femoral veins were observed. Under the actions of repeated chest compressions at intervals of 2–3 s in the freshly dead rats, the contraction and dilation of the heart were found to cause the same pulsatile flow of the adventitial ISF (Figure 4A), while the venous pressure was 1–2 mmHg (Table S3). When the chest cavity opened and the atria or ventricles were compressed at an interval of 10–15 s, it was found that every compression of the atria (Figures 4B and 4B1) or ventricles (Figures 4C and 4C1) induced a centrifugal motion of the adventitial ISF, and every dilation of the atria (Figures 4B and 4B2) or ventricles (Figures 4C and 4C2) caused a centripetal motion, while the venous pressure was 1–2 mmHg (Table S3). In one respiratory cycle, the expansion of the lungs during inspiration caused the adventitial ISF to move centrifugally (Figures 4D and 4D1), while the contraction of the lungs during expiration caused a centripetal movement of the adventitial ISF (Figures 4D and 4D2). The venous pressure was measured to be 0–1 mmHg under such one-shot ventilation (Table S3).

### Illustration of the effects of the repeated cardiac compressions or ventilations on the adventitial flow in freshly dead rats with opened ventricular chambers

In the dead rats with open ventricular chambers, no blood flow from the apex was observed during the experiments, whether by repeated cardiac compressions or mechanical ventilations of lungs. Meanwhile, the measured arterial and venous blood pressures were

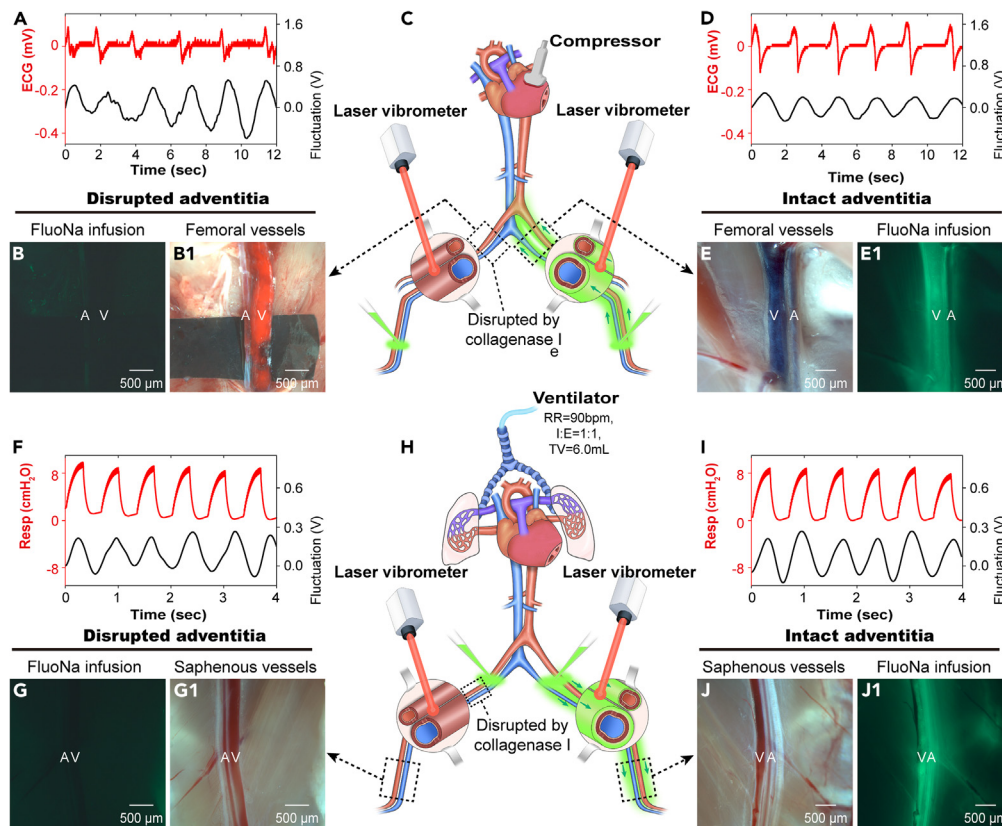


**Figure 5. Illustration of the effects of the repeated cardiac compressions or ventilations on the adventitial flow in freshly dead rats with opened ventricular chambers**

In the freshly dead rats, the apex of the heart was cut open to air so that the repeated cardiac compressions or ventilations cannot induce blood flow, and the mechanical motions of the vessel wall was detected by a laser vibrometer. The adventitial pathways along the right femoral vessels were disrupted by collagenase I, while the left remained intact (C and H). After the FluoNa was infused into the adventitial pathways on distal saphenous vessels of both sides, the heart was compressed repeatedly at 30–60bpm for 30 min in 6 rats while the lungs were not ventilated (C).

(H) showed that the lungs were ventilated (RR 90bpm, I/E 1:1, TV 6.0 mL) for 30 min in another 6 rats while the heart was not compressed after the FluoNa was infused into the adventitial pathways on the proximal femoral vessels of both sides.

(B and B1) The distal FluoNa cannot flow centripetally through the right disrupted adventitial pathways.

(E and E1) The distal FluoNa flowed centripetally and stained the intact adventitial pathways along the left femoral vessels.

(G and G1) The proximal FluoNa cannot flow centrifugally through the right disrupted adventitial pathways.

(J and J1) The proximal FluoNa flowed centrifugally and stained the intact adventitial pathways along the left saphenous vessels.

(A, D, F, and I) The mechanical motions were detected on the wall of both the right (A) and the left (D) femoral vessels. A, artery, V, vein.

$10.3 \pm 2.3/4.9 \pm 0.5$  mmHg and  $0.7 \pm 0.1$  mmHg by cardiac compressions, or  $3.8 \pm 1.0/3.7 \pm 1.0$  mmHg and  $0.6 \pm 0.3$  mmHg by ventilations, respectively (Figure S6). However, under repeated cardiac compressions, it was observed that the distal FluoNa was able to flow centripetally along the left femoral vessels but could not pass through the adventitial pathways of the right femoral vessels, which were disrupted by collagenase I (Figures 5B, 5B1, 5E, and 5E1). In contrast, under repeated ventilation of the lungs, the proximal FluoNa was observed to flow centrifugally along the left femoral vessels, but not through the adventitial pathways of the right femoral vessels, which had been disrupted by collagenase I as well (Figures 5G, 5G1, 5J, and 5J1). Moreover, even if the cardiac compressions or ventilations of the lungs could cause the mechanical fluctuations in the vascular walls of the lower limbs, the FluoNa in the adventitial pathways can flow centripetally driven by the heart or centrifugally driven by the lungs, respectively (Figures 5A, 5D, 5F, and 5I).

When the root of the main pulmonary artery was clamped, the expansion and contraction of the lung can still cause the to-and-fro motions of the adventitial ISF along the femoral vein. However, after clamping of the thoracic segment of the inferior vena cava, the movements of the adventitial ISF along the femoral vein disappeared. These results suggested that effects of the lungs' expansions and contractions on the adventitial ISF flow along the femoral venous vessels were achieved through the pulmonary venous vessels, rather than the pulmonary arteries.

### Qualitative observations on adventitial ISF flow pathways along the systemic and pulmonary arteries and veins by FluoNa

For the systemic vasculature, the adventitia-infused FluoNa from the right lower limb was found to stain the adventitial connective tissues of inferior vena cava (Figures S7E–S7G), aorta (Figures S7B–S7D), and the heart muscles of the left ventricle (Figure 6B). The FluoNa infused into

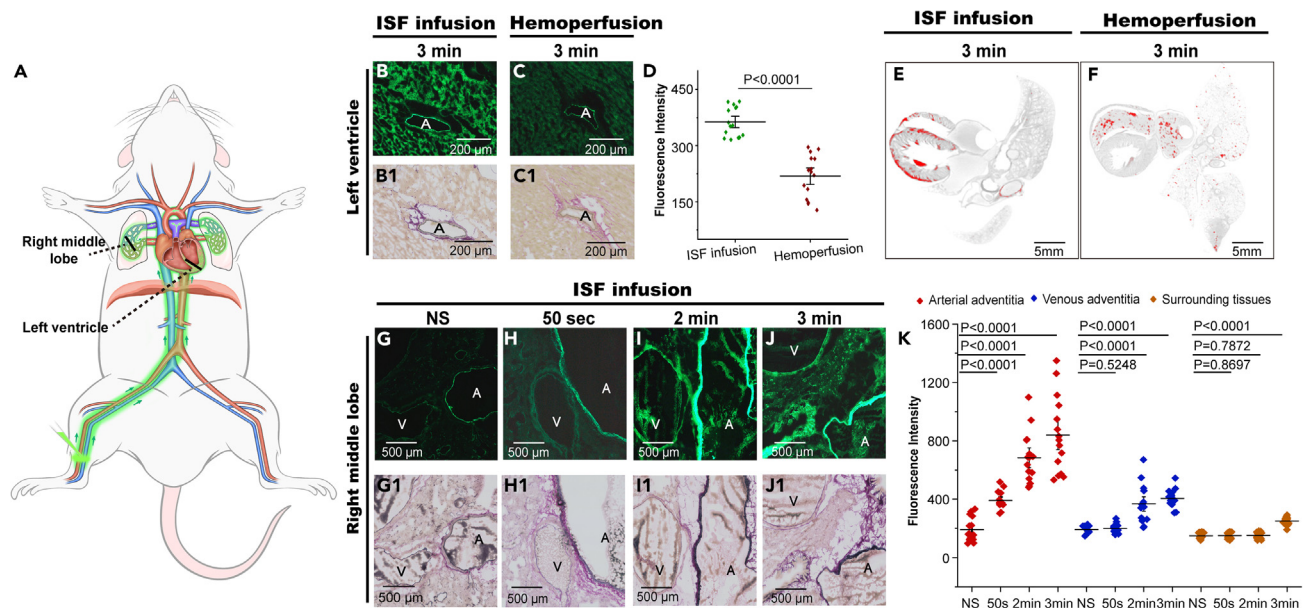


**Figure 6. Qualitative observations on adventitial ISF perfusion and intravenous perfusion of the FluoNa or silver nitrate into the heart, and the circulatory cycle of adventitial ISF along the pulmonary vasculature**

At 3 min after the adventitial infusion of FluoNa from the adventitial pathways of the lower limb or the intravenous injection of FluoNa, the fluorescence intensity (B) of the myocardial tissues near the left ventricular epicardium by adventitial infusion (A) was significantly stronger than those by intravenous injection (C). (B1–C1) were the bright field corresponding to (B and C). By SMCT, the silver nitrate (red) from the adventitial pathways of the lower limb was found in the left and right ventricular muscles near the left and right ventricular epicardium (E) significantly but few in the lungs. In contrast, the silver nitrate by intravenous injection was found inside the right ventricle, some coronary arteries, and pulmonary vessels (F). To delineate the adventitial ISF cycle of the pulmonary vasculature, FluoNa was infused into the adventitial pathways of the lower limbs and detected in the middle lobe of the right lung at different times.

(G and G1) The cross-sections showed a pulmonary artery and vein in the middle lobe and sampled at 50 s after the adventitial infusion of NS.

(H and H1) At 50 s after the adventitial infusion, the distal FluoNa stained the adventitial pathway of the pulmonary artery but not the adventitial pathways of the vein and the perivascular tissues.

(I and I1) At 2 min after the adventitial infusion, the distal FluoNa stained the adventitial pathway of the pulmonary artery and vein but not the perivascular tissues.

(J and J1) At 3 min after the adventitial infusion, the distal FluoNa stained the adventitial pathway of the pulmonary artery and vein and the perivascular tissues.

(K) The changes of the fluorescence intensity of the adventitial pathways in arteries, veins and the surrounding tissues, respectively. The findings indicated that the adventitial ISF flow cycle along the pulmonary vasculature is from the heart to the lungs along the pulmonary arteries, and from the lungs to the heart along the pulmonary veins. In (D and K), t test, mean  $\pm$  SEM, n = 3 rats. A, artery. V, vein. The sites of cross section in in heart (B and C) and lung (G–J) were pointed at (A) as the black solid lines.

the adventitial pathways of the right axillary artery and vein (Figures S7K–S7M), and the left carotid artery (Figures S7H–S7J) was found to have stained the right anterior vena cava (Figure S7N–S7P), aorta, and the heart. These data suggested that the adventitial ISF flow in the adventitial pathways centripetally along both arteries and veins of the systemic vasculature into the heart.

For the pulmonary vasculature, it was also found that the adventitial FluoNa could move along the pulmonary artery toward the lungs (Figures S8A and S8A1) or along the pulmonary vein toward the heart (Figures S8B and S8B1). The findings indicated that the adventitial ISF flow cycle along the pulmonary vasculature was from the heart into the lungs via the pulmonary arteries and back to the heart via the pulmonary veins.

For the coronary arteries of the heart, the FluoNa, that was infused into the superficial tissues on the ventricular apex, was found to flow in the adventitial pathways along the coronary arteries toward the base of the heart (Figure S10A–S10C, Video S9), suggesting that the upper part of the heart above the coronary sulcus might be the driver for the adventitial ISF flow along the coronary arteries of the ventricles.

### Qualitative observations on adventitial ISF perfusion and intravenous perfusion of the FluoNa or silver nitrate into the heart, and the circulatory cycle of adventitial ISF along the pulmonary vasculature

The distributions in the myocardium of the adventitial infused tracers from the lower limbs were studied by the FluoNa or silver nitrate, respectively. At 3 min after the administration of the FluoNa into the adventitia of saphenous vessels in lower limb, it was found that the fluorescence intensity in the myocardium (Figures 6B and 6B1) by the adventitial infusion of the FluoNa was stronger than that of hemoperfusion by intravenous injection at 3 min (Figures 6C and 6D). The SMCT showed that the silver nitrate from the adventitial pathways along the saphenous vessels have entered the ventricular muscles (Figures 6E and Video S10), the amount of which was much more than those by hemoperfusion

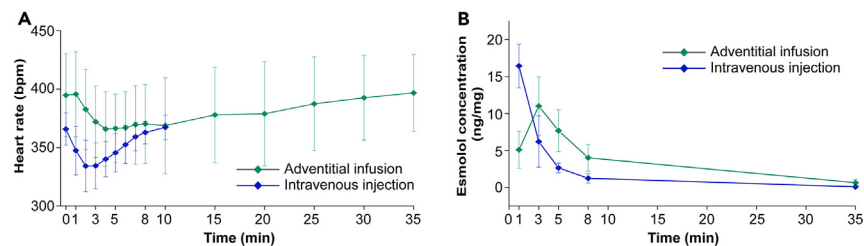


**Figure 7. Reduction of the HR with Esmolol by adventitial infusion and intravenous injection**

(A) The adventitial Esmolol caused a slow HR reduction at 1 min after the infusion. The maximum reduction was at 4 min, and the HR began to recover after 8–10 min. In contrast, the intravenous Esmolol induced a rapid HR reduction immediately after the injection. The maximum reduction was at 2 min, and the HR began to recover at 3 min.

(B) Detected by LC-MS/MS, the Esmolol concentration of intravenous injection increased rapidly and reached the peak at 1 min. The Esmolol concentration of adventitial infusion increased slowly and reached the peak at 3 min.

(Figure 6F). In addition, the silver nitrate from the adventitial pathways was mainly distributed in the subepicardial tissues. However, how to identify the adventitial ISF from the systemic vasculature circulate throughout the heart still needs more research.

### Qualitative observations on the adventitial ISF flow starting from the ends of the systemic vasculature, and the circulatory pathways of adventitial ISF from pulmonary arteries to veins by FluoNa

Does the adventitial ISF flow only under pathological conditions like extremity edema, or is it an inherent flow under physiological conditions? Using conventional angiography, we found that even without administration of the FluoNa directly into the adventitial pathways, the FluoNa from arterial blood still stained the adventitial pathways along both the femoral vein and artery after capillary exchange in the distal lower limb (Video S11). The results suggested that the ISF near capillaries would flow into both arterial and venous adventitial pathways after filtered from capillary walls of the systemic vasculature.

To explore how the adventitial ISF along the pulmonary arteries entered the adventitial pathways along the pulmonary veins, we studied the temporal distribution characteristics of the adventitial FluoNa in the middle lobe of right lung where a pair of adjacent artery and vein could be found. At 50 s after the adventitial infusion of the FluoNa into the adventitial pathways of the saphenous vessels, the adventitial pathway of the pulmonary artery was stained but the adventitial pathways of the vein and the perivascular tissues were not (Figures 6H, 6H1, and 6K). This is significantly different from the results of hemoperfusion at 50 s after the intravascular FluoNa (Figures S9A–S9C). Then, at 2 min, the adventitial pathways of both the pulmonary artery and vein were stained (Figures 6I, 6I1, and 6K); at 3 min, the adventitial pathways of the pulmonary artery and vein as well as the perivascular tissues in between have been stained together (Figures 6J, 6J1, and 6K). These results showed that the adventitial ISF along the pulmonary artery would enter the adventitial pathways along the pulmonary vein when an artery meets an adjacent vein.

### Effects of heart-targeted drug delivery for an adventitial ISF flow pathway

The potential function of the adventitial pathways as a novel route for drug delivery targeting the heart was explored. The effects on HR reduction in adventitial infusion group was found to be slower than that in intravenous injection group at 1–3 min after the administration (Figure 7A). The changes of Esmolol concentration detected in the myocardium of the ventricular apex coincided with the changes of the HR reduction by either adventitial infusion or intravenous injection (Figure 7B). The Esmolol concentration in myocardium of intravenous injection increased rapidly and reached the peak at 1 min after administration. The Esmolol concentration in myocardium by adventitial infusion reached the peak at 3 min and remained higher than that by intravenous injection starting from 3 min after administration.

## DISCUSSION

Building on previous findings on the long-range adventitial ISF flow along the larger-caliber vessels and its connections with the heart and lungs,<sup>22–25</sup> our current experiments further identified that the ISF flows in adventitial matrix surrounded by layers of fascia (Figures 2M, 2M1, 2O, 2O1, 2Q, S2A–S2C, and S3B–S3D) and centripetally along the major arteries and veins of the systemic vasculature to the epicardium and myocardium (Figures S1 and S7), then into the lungs via the pulmonary arteries and returns the heart via the pulmonary veins (Figure S8), which is neither perivascular tissues nor blood or lymphatic vessels. The driving mechanism of such adventitial ISF flow was found to be regulated by the heart and lungs and elucidated in the physiological or non-physical conditions of the rat model. Under physiological conditions of rats, the measured velocity of the speckle-like adventitial ISF flow along the femoral veins was positively correlated with HR, increased when holding breath, and became pulsative during heavy breathing. During respiratory cycle, each expansion of the lungs during inflation generates a centrifugal flow of adventitial ISF, while each contraction of the lungs during deflation generates a centripetal adventitial ISF flow. During cardiac cycle, each dilation of atria or ventricles generates a centripetal flow of adventitial ISF, while each contraction of atria or ventricles generates a centrifugal adventitial ISF flow. By repeated compressions of atrium or ventricles of the heart without respiration, the adventitial

ISF was driven to flow centripetally along the femoral vessels (Figures 5A–5E1). By repeated ventilations of lungs without heartbeat, the adventitial ISF was driven to flow centrifugally along the femoral vessels (Figures 5F–5J1). It seemed that a respiratory movement of the lungs is able to retard the centripetal flow of adventitial ISF generated by the beating heart. As to the exchange with blood circulation, the ISF was found to flow longitudinally in the adventitial pathways along the vascular vessels, diffuse into the perivascular connective tissues, and return to blood circulation through the adjacent blood capillaries and lymphatic vessels during the long-range transport processes of either rats or rabbits.<sup>9,25,36</sup> The detailed mechanism to maintain mass fluid balance among such an ISF transport, spread and redistribution system, blood circulation and lymphatic system requires more research. Here, our findings propose that the heart and lungs work together to drive the adventitial ISF to flow centripetally along the major systemic arteries and veins, and circulate around the pulmonary vasculature, comprising an adventitial ISF circulatory network, abbreviated as adventitial ISF circulation. Further identification of adventitial pathways along the arterioles, venules, and capillaries in the lungs and other organs or tissues will provide the missing link to adventitial ISF cycle. How such regulative mechanisms of heartbeat and respiration on adventitial ISF flow via vasculature takes a role in modulating the ISF flow around cells or capillaries of tissues or organs, or blood and CSF in brain needs more studies.<sup>18–21</sup>

### The adventitial pathways were neither blood and lymphatic vessels nor the passageways in perivascular spaces

The adventitial pathways are the outermost connective tissues covering of vessels and neither blood and lymphatic vessels nor the passageways perivascular spaces in perivascular spaces.<sup>22,25</sup> Even if the perivascular tissues were stripped, the ISF was still found to flow longitudinally along the vessels in the remaining adventitial tissues by the fluorescent tracer (Figures S2B, S2B1, and S3A–S3D1). When the remaining adventitial tissues were disrupted by collagenase I, the longitudinal flow of the fluorescent adventitial ISF along the vessels would be interrupted while the intravascular lumen was unobstructed (Figures 2B–2D, 2E, 2M, 2M1, 2O, 2O1, S2B–S2C1). Under the real-time stereofluorescence microscopy, the movement of the FluoNa in the longitudinal fluorescent lines along the side of the venous vessel clearly illustrated the continuous ISF flow in the remaining adventitial tissues (Figures 2B and 2C, Video S5). As analyzed by real-time frozen sections, the adventitial pathways for the ISF flow, that were stained by the flow of the FluoNa from the distal (Figures S2B, S2B1, and S3A–S3D1), consisted of the outermost layer of fascia and the inner adventitial matrix, covering the media of either arterial or venous vessels. Unlike the conduit-like passageways in perivascular spaces next to the small intracranial vessels,<sup>37</sup> the intrinsic structures of the adventitial pathways were composed of adventitial matrix, within which, the micro-CT found that there were approximate 2300–2800 fibers inside the femoral arterial or venous adventitial pathways, respectively (Figure 2Q). However, neither fibers nor gel-like substances within adventitial matrix can flow freely along the vessels over a long distance. Hence, the boundary structures for adventitial ISF flow longitudinally along the vessels were the outermost layers of fascia and innermost tunica media of blood vessels. We named this adventitial ISF flow pathway “interstitial matrix-membranes channel, abbreviated as matrix channel”.<sup>9,24,25,38</sup> Fluid flow in matrix channel is named matrix flow. In addition to adventitial pathways, identifying a diverse anatomical distribution of such non-conduit-like channels in animals and humans is extremely fascinating.

The observed flow of adventitial ISF at different velocities suggested complex structures in the adventitial pathways as well. Within 20 s after adventitial infusion, fluorescein began to enter the adventitial channels, and the observed early rapid flow of the FluoNa represented a fast internal channel in the adventitial pathways. The subsequent speckle-like flow represented a slow internal channel in the adventitial pathways. Nevertheless, our current imaging techniques cannot further differentiate between the multiple fluorescein flow in these different internal channels. It is needed to develop a dynamic high-speed fluorescence imaging technology with higher resolution to visualize such diverse ISF flow in an adventitial pathway with multiple internal channels.

### The regulatory mechanism of adventitial ISF flow by the heartbeat and respiration

The dynamic patterns of the heart and lungs to regulate the adventitial ISF flow are unique. By measuring the motions of fluorescent speckles along the femoral veins under physiological conditions (Video S5), we found that the flow rate of adventitial ISF was positively correlated with the HR (Figure 3B). The flow velocity of adventitial ISF increased during apnea and fluctuated by heavy breaths, and its fluctuation frequency was consistent with the breath rate (Figures 3C and 3C1). By ventilation, it was showed that a large TV can cause a pulsed centripetal flow of adventitial ISF in alive rats (Figures 3C1 and 3F1), while a pulsed centrifugal flow in dead rats (Figure 3G1). By adjusting different parameters of mechanical ventilation in alive or dead rats, it was displayed that the frequency of the pulsed flow rate of the adventitial ISF was consistent with the RR (Figures 3D, 3D1, 3E, 3E1); the inspiration and expiration (I/E) ratio (1:1, 2:1, 1:2) determined the descending and ascending branches of the velocity pulse (Figures 3H, 3H1, 3I, and 3I1). These findings showed the correlations between the changes in the adventitial ISF velocity and the heartbeat and respiration, clearly demonstrating that the adventitial ISF flow along the femoral vein was a synergistic result of the heart and lungs.

In our experimental observations, when the TV of ventilation was less than 3 mL, almost no effect of breathing on the adventitial ISF flow rate can be found. When the TV was greater than 4 mL, it can be displayed that the flow rate fluctuated with respiration. The proposed empirical dynamic Equation 3 further illustrated the correlations of the adventitial ISF flow rate in an adventitial pathway with the cyclical motions generated by the regular heartbeats and irregular respirations (Figures 3J–3L, Videos S6, S7, and S8, Note S1). In the present study, the continuous *T* represented the HIT of adventitial pathways along the femoral veins, while the fluid transportability of diverse adventitial pathways in other parts of various animals and humans requires further explorations. In addition, the greater TV will increase thoracic pressure as well. Future research on the relationship between pressure and fluctuated flow rate may further modify this equation.<sup>19,20</sup>

The continuous cyclical diastolic and contractive motions of the heart and lungs were responsible for the to-and-fro flow of adventitial ISF. So how does each heartbeat or breathing motion of the lungs affect the adventitial ISF flow?

### The proposed driving mechanisms of the heart and lungs regulating the adventitial ISF flow

To clarify the effects of each heartbeat or breath on the flow of adventitial ISF during cardiac or respiratory cycle, we performed experiments in dead rats by means of chest compressions, open-chest atrial or ventricular compressions, and mechanical ventilation, respectively. It was found that the speckle-like adventitial ISF along the femoral vein was “pulled” toward the heart when the atria (Figure 4B2) or ventricles (Figure 4C2) diluted, or the lungs (Figure 4D2) contracted, whereas the adventitial ISF was “pushed” away from the heart when the atria (Figure 4B1) or the ventricles (Figure 4C1) contracted, or the lungs (Figure 4D1) expanded. In freshly dead bodies of rats, repeated mechanical cardiac compressions can drive the adventitial ISF to move back and forth, and overall flow toward the heart (Figures 4A and 5C). In contrast, repeated mechanical ventilations drove the adventitial ISF to move back and forth, and overall flow centrifugally along the femoral vein (Figure 5H and Video S8). Due to the lack of quantitative observation methods of fluid flow in an arterial adventitial pathway, future studies are needed to reveal the effects of each stroke of the heart and lungs on the adventitial ISF flow along the systemic arteries as well as the pulmonary arteries and veins.

The mechanisms that every cyclical deformation of either the heart or lungs generates a pair of to-and-fro driving forces to “pull” or “push” the ISF to flow in the adventitial pathways along the systemic and pulmonary vascular tree are fascinating. Is it the perivascular pump driving the ISF to flow in the PVS of brain? There are two hypothesized causes of the perivascular pump, one is the shear force generated by the pulsating blood flow on the vessel wall, and the other is the mechanical pulsation generated after the heartbeat is transmitted through the rigidly connected vessel walls.<sup>37,39</sup> To investigate the effects on the adventitial ISF flow by the pulsating blood flow and the mechanical pulsations of the vessel walls, we constructed an animal model with open ventricular chambers in air and meanwhile, the mechanical motions of the femoral vessel walls were detected by a laser vibrometer. Whether by repeated cardiac compressions or mechanical ventilations of lungs, no blood flow from the apex was observed during the experiments, while the measured arterial and venous pressure were almost close to zero and significantly lower than the physiological arterial and venous pressures (Figure S6; Table S3). Under repeated cardiac compressions, the distal FluoNa was able to flow centripetally along the left femoral vessels (Figures 5B, 5B1, 5E, and 5E1). In contrast, the proximal FluoNa was driven to flow centrifugally along the left femoral vessels by repeated ventilation of the lungs (Figures 5G, 5G1, 5J, and 5J1). Moreover, we also found that the mechanical fluctuations of the vessel walls did not determine whether the FluoNa in the adventitial pathways flowed centripetally or centrifugally (Figures 5A, 5D, 5F, and 5I). Hence, these data showed that the driving forces for the continuous adventitial ISF flow come mainly from the expansions and contractions of the heart or lungs, rather than from the continuous pulsating blood flow or mechanical motions of the vessel walls. Of course, the other physiological factors that might involve in the adventitial ISF flow, such as the shear stress of blood flow, cardiac contractile strength, muscle contraction along the transport pathways, etc., need to be studied in the subsequent research.

Based on our previous and current findings,<sup>22,24,25,29,40</sup> a working hypothesis was proposed to understand the mechanisms of the expansions and contractions of the heart and lungs “pull” or “pushing” the adventitial ISF flow centripetally or centrifugally along the femoral vessels: (1) When the heart and lungs expand or contract, the interstitial matrix within the heart and lungs will deform cyclically and work as a driver, named as “matrix or gel pump”. (2) The deformations of either cardiac or pulmonary matrix pump can generate at least two driving forces, the pressure gradients, and the fluctuating interfacial interaction forces of fluid in the diverse interspaces inside matrix.<sup>25</sup> (3) The positive or negative pressure gradients generated by the atrial or ventricular matrix contracted, or the pulmonary matrix expanded will drive the adventitial ISF to flow along the vascular tree away from the driver or toward the driver. (4) Mediated by the intact adventitial tissues, the fluctuating interfacial interaction forces generated by the atrial or ventricular matrix diluted, or the pulmonary matrix contracted will “pull” the adventitial ISF to flow along the vascular tree toward the driver.<sup>24,25</sup> In the human cadaver experiments, the “cardiac matrix pump” that was repeatedly compressed by an automatic cardiac compressor, had “pulled” the peripheral ISF in the thumb via the adventitial pathways into the epicardium.<sup>24</sup> In alive rabbits, the “cardiac matrix pump” had “pulled” the peripheral ISF via the adventitial pathways into the heart and entered the pericardial cavity, causing pericardial effusion.<sup>22,25</sup> As future works, the driving mechanisms of cardiac and pulmonary matrix pumps and the kinematics of adventitial pathways require more explorations.

As for the functions delivering fluid and dissolved constituents, we found that the adventitial infusion is significantly different from intravenous injection for drug delivery. The effects on the HR reduction of Esmolol by adventitial infusion was a slow and longer-drug-effect pattern compared to the rapid reduction by the intravenous injection (Figure 7A). It was also found that the concentration of adventitial Esmolol was higher than that of intravenous Esmolol at 3, 5, 8 min, respectively (Figure 7B). If Esmolol had been inside blood vessels, Esmolol would have been rapidly metabolized to inactive products by hydrolysis of the intraerythrocytic esterases in red blood cells.<sup>41</sup> The detected higher concentration of Esmolol in the ventricular tissues indicated that the adventitial infused Esmolol probably entered the myocardium through a fluid transport pathway that does not contain red blood cells. The presented pilot study may inspire the heart-targeted extravascular route of drug delivery in the future, especially for the drugs that seek to avoid rapid metabolism by erythrocytes.

In summary, our current findings showed that the heart and lungs play a synergistical role in regulating the ISF flow along the adventitia of vasculature throughout the body. The relationship of adventitial ISF flow with those around capillaries, and their mechanisms to maintain the homeostasis of internal environment between cells of diverse tissues or organs are particularly intriguing. The proposed matrix pump might inspire further research on the driving mechanisms of how the heart and lungs generate the forces of “pull” or “push” during a cardiac or pulmonary cycle. Under the actions of heartbeat and respiration, the centripetal to-and-fro flow of adventitial ISF along the systemic blood vessels may simultaneously participate in the perfusion and drainage of the ISF into and out of organs or tissues. For pulmonary circulation, the influence of the circulatory flow of adventitial ISF on the physiological and pathophysiological functions of the heart and lungs is a new research topic. Elucidating the relationship between adventitial ISF flow and vascular physiological functions and diseases will be an important advance in vascular biology. A specialized imaging technique is needed to study adventitial ISF flow along arteries. For drug delivery targeting the heart and lungs, the studies on the unique drug metabolism characteristics of adventitial ISF circulatory pathways may facilitate

a novel therapeutic strategy for extravascular drug delivery and pharmaceuticals. For human health and diseases, further studies on ISF circulation will bring innovations in the fields of medical applications. For example, clarifying the ratio of myocardial tissues perfusion by adventitial ISF flow and traditional blood perfusion will provide a new therapeutic method for myocardial infarction, a new tunica-angiography via adventitial ISF flow by MRI or other medical imaging technique will bring fruitful insights into vascular diseases, and comprehensive studies on the impact of cardiopulmonary motions on the to-and-fro flow of adventitial ISF and CSF will contribute to understand the perfusion and drainage patterns of the ISF in diverse tissues or organs throughout the body, likely inspiring treatments for Alzheimer's disease, amyloid deposition diseases, pulmonary fibrosis, connective tissue diseases, etc.

### Limitations of the study

1. Together with our previous studies, it was found that the ISF around the vascular vessels will enter the adventitial matrix-membranes channels, the lumen of blood and lymphatic vessels in the meanwhile. Future studies should clarify the proportion of the ISF entering the diverse channels under physiological conditions.
2. Regulated by the heartbeat and respiration, the specific physiological and pathological functions of such an adventitial ISF circulatory network need further studies. In particular, the functions of the to-and-fro flow of adventitial ISF along vasculature need more explorations, such as whether it participates in the perfusion and drainage of the ISF into and out of organs or tissues via vasculature.
3. The mechanical mechanism by which the cyclic motion of the heart and lungs drives the to-and-fro movement of adventitial ISF needs to be clarified.
4. Limited by the current imaging methods, the flow velocity of adventitial ISF in arterial matrix-membranes channel along the systemic and pulmonary vasculature needs further studies.
5. For pulmonary circulation, how the dilation and contraction of either atria or ventricles, and the expansion and relaxation of the lungs cause the adventitial ISF to flow to-and-fro still requires further studies, especially for the flow directions of adventitial ISF along pulmonary arteries or veins under various physiological conditions.
6. For the heart, the distributions and flow directions of the adventitial ISF along the arteries and veins of atria and ventricles need to be identified. In addition, how adventitial ISF from systemic or pulmonary vasculature flows into or out of the right and left atria or ventricles requires more research.
7. Consistent with our previous studies, the current data have verified that the structures for adventitial ISF flow are the adventitial matrix paved by layers of fascia, within which, how to identify the complex spaces within these matrix-membranes channels for diverse fluid flow requires more imaging technique.

### STAR★METHODS

Detailed methods are provided in the online version of this paper and include the following:

- **KEY RESOURCES TABLE**
- **RESOURCE AVAILABILITY**
  - Lead contact
  - Materials availability
  - Data and code availability
- **EXPERIMENTAL MODEL AND STUDY PARTICIPANT DETAILS**
  - Animals
- **METHOD DETAILS**
  - The selection of the imaging tracers
  - Adventitial infusion and intravenous injection
  - Image acquisition by MRI
  - *In vivo* fluo-imaging of adventitial pathways in limb
  - Measuring rapid and speckle-like flow rate
  - Qualitative observation on circulatory pathways
  - *Ex vivo* fluo-imaging and histological analysis
  - Effects of heartbeat or breath on adventitial flow
  - Cardiac compression or ventilation on ISF flow
  - Distributions of silver nitrate in tissues by SMCT
  - Adventitial matrix of femoral vessels by micro-CT
  - Esmolol experiments in myocardium analysis
- **QUANTIFICATION AND STATISTICAL ANALYSIS**

### SUPPLEMENTAL INFORMATION

Supplemental information can be found online at <https://doi.org/10.1016/j.isci.2024.109407>.

## ACKNOWLEDGMENTS

We thank Professors Guanhua Xu, Yixin Zeng, and Kaixian Chen, Weiwu Hu, Bo Song, Saicang Lobsang Hwardan Chegynima, Jamyang Danchour, Angwen zhabar, Andreas Sammer, and Georg Feigl for their fruitful discussions. We thank Weihua Wang, Fang Wei, Yu Tang in center of pharmaceutical technology of Tsinghua University for their help in LC-MS/MS.

Sources of Funding: This work was supported by National Natural Science Foundation of China (82050004), Innovation Team and Talents Cultivation Program of National Administration of Traditional Chinese Medicine. (No: ZYYCXTD-D-202202), and Beijing Hospital Clinical Research 121 Project (121-2016002).

## AUTHOR CONTRIBUTIONS

Hongyi.L. conceived and developed the original ideas, concepts and theory of interstitial fluid circulatory network. Hongyi.L., H.L., C.M., and F.J. designed the experiments. Hongyi.L. wrote the paper. B.L., W.L., X.Q., Hongyi.L., J.L., Z.H., X.Y., and D.H. performed the experiments. Y.H., B.L., and H.L. calculated the velocity. Hongyi.L., H.L., Y.H., and B.L., carried out the empirical formula. J.Z., Hongyi.L., B.L., and T.L., performed the MRI experiments. B.L., C.Y., Z.L., and T.G. performed the spectral micro-CT experiments. Hongyi.L., C.M., F.J., J.H., and Z.Z. analyzed the imaging data. Wenqing.L., Hongyi.L., F.W., and L.L. analyzed the data for drug delivery experiments. Hongyi.L. and B.L. prepared pictures and videos.

## DECLARATION OF INTERESTS

The authors declare no competing interests.

Received: December 6, 2023

Revised: January 29, 2024

Accepted: February 29, 2024

Published: March 4, 2024

## REFERENCES

1. Woollam, D.H., and Millen, J.W. (1955). The perivascular spaces of the mammalian central nervous system and their relation to the perineuronal and subarachnoid spaces. *J. Anat.* 89, 193–200.
2. Hatton, G.I. (1988). Pituicytes, glia and control of terminal secretion. *J. Exp. Biol.* 139, 67–79. <https://doi.org/10.1242/jeb.139.1.67>.
3. Kendall, M.D. (1989). The morphology of perivascular spaces in the thymus. *Thymus* 13, 157–164. <https://doi.org/10.1007/bf02694455>.
4. Edelman, E.R., Nugent, M.A., and Karnovsky, M.J. (1993). Perivascular and intravenous administration of basic fibroblast growth factor: vascular and solid organ deposition. *Proc. Natl. Acad. Sci. USA* 90, 1513–1517. <https://doi.org/10.1073/pnas.90.4.1513>.
5. Pollock, H., Hutchings, M., Weller, R.O., and Zhang, E.T. (1997). Perivascular spaces in the basal ganglia of the human brain: their relationship to lacunes. *J. Anat.* 191 (Pt 3), 337–346. <https://doi.org/10.1046/j.1469-7580.1997.19130337.x>.
6. Iloff, J.J., Wang, M., Liao, Y., Plogg, B.A., Peng, W., Gundersen, G.A., Benveniste, H., Vates, G.E., Deane, R., Goldman, S.A., et al. (2012). A paravascular pathway facilitates CSF flow through the brain parenchyma and the clearance of interstitial solutes, including amyloid beta. *Sci. Transl. Med.* 4, 147ra111. <https://doi.org/10.1126/scitranslmed.3003748>.
7. Morrison, S.J., and Scadden, D.T. (2014). The bone marrow niche for haematopoietic stem cells. *Nature* 505, 327–334. <https://doi.org/10.1038/nature12984>.
8. Wardlaw, J.M., Benveniste, H., Nedergaard, M., Zlokovic, B.V., Mestre, H., Lee, H., Doubal, F.N., Brown, R., Ramirez, J., MacIntosh, B.J., et al. (2020). Perivascular spaces in the brain: anatomy, physiology and pathology. *Nat. Rev. Neurol.* 16, 137–153. <https://doi.org/10.1038/s41582-020-0312-z>.
9. Pirri, C., Wells, R.G., De Caro, R., Stecco, C., and Theise, N.D. (2023). What's old is new again: The anatomical studies of Franklin P. Mall and the fascial-interstitial spaces. *Clin. Anat.* 36, 887–895. <https://doi.org/10.1002/ca.24019>.
10. Casley-Smith, J.R. (1976). Calculations relating to the passage of fluid and protein out of arterial-limb fenestrae, through basement membranes and connective tissue channels, and into venous-limb fenestrae and lymphatics. *Microvasc. Res.* 12, 13–34. [https://doi.org/10.1016/0026-2862\(76\)90003-0](https://doi.org/10.1016/0026-2862(76)90003-0).
11. Hauck, G. (1982). The connective tissue space in view of the lymphology. *Experientia* 38, 1121–1122. <https://doi.org/10.1007/bf01955400>.
12. Butler, T.P., Grantham, F.H., and Gullino, P.M. (1975). Bulk transfer of fluid in the interstitial compartment of mammary tumors. *Cancer Res.* 35, 3084–3088.
13. Pathak, A.P., Artemov, D., Ward, B.D., Jackson, D.G., Neeman, M., and Bhujwalla, Z.M. (2005). Characterizing extravascular fluid transport of macromolecules in the tumor interstitium by magnetic resonance imaging. *Cancer Res.* 65, 1425–1432. <https://doi.org/10.1158/0008-5472.Can-04-3682>.
14. Hall JE, G.A. (2011). The microcirculation and lymphatic system. In Guyton and Hall Textbook of Medical Physiology, 12th Ed.
15. Sawdon, M., and Kirkman, E. (2017). Capillary dynamics and the interstitial fluid-lymphatic system. *Anaesth. Intensive Care* 18, 309–315.
16. Hadaczek, P., Yamashita, Y., Mirek, H., Tamas, L., Bohn, M.C., Noble, C., Park, J.W., and Bankiewicz, K. (2006). The “perivascular pump” driven by arterial pulsation is a powerful mechanism for the distribution of therapeutic molecules within the brain. *Mol. Ther.* 14, 69–78. <https://doi.org/10.1016/j.ymthe.2006.02.018>.
17. Gan, Y., Holstein-Rønsho, S., Nedergaard, M., Bostter, K.A.S., Thomas, J.H., and Kelley, D.H. (2023). Perivascular pumping of cerebrospinal fluid in the brain with a valve mechanism. *J. R. Soc. Interface* 20, 20230288. <https://doi.org/10.1098/rsif.2023.0288>.
18. Daouk, J., Bouzerar, R., and Baledent, O. (2017). Heart rate and respiration influence on macroscopic blood and CSF flows. *Acta Radiol.* 58, 977–982. <https://doi.org/10.1177/0284185116676>.
19. Laganà, M.M., Di Tella, S., Ferrari, F., Pelizzari, L., Cazzoli, M., Alperin, N., Jin, N., Zacà, D., Baselli, G., and Baglio, F. (2022). Blood and cerebrospinal fluid flow oscillations measured with real-time phase-contrast MRI: breathing mode matters. *Fluids Barriers CNS* 19, 100. <https://doi.org/10.1186/s12987-022-00394-0>.
20. Baselli, G., Fasani, F., Pelizzari, L., Cazzoli, M., Baglio, F., and Laganà, M.M. (2022). Real-time phase-contrast MRI to monitor cervical blood and cerebrospinal fluid flow beat-by-beat variability. *Biosensors* 12, 417. <https://doi.org/10.3390/bios12060417>.
21. Töger, J., Andersen, M., Haglund, O., Kylkilahti, T.M., Lundgaard, I., and Markenroth Bloch, K. (2022). Real-time imaging of respiratory effects on cerebrospinal fluid flow in small diameter passageways. *Magn. Reson. Med.* 88, 770–786. <https://doi.org/10.1002/mrm.29248>.
22. Li, H.Y., Chen, M., Yang, J.F., Yang, C.Q., Xu, L., Wang, F., Tong, J.B., Lv, Y., and Suonan, C. (2012). Fluid flow along venous adventitia in rabbits: is it a potential drainage system complementary to vascular circulations? *PLoS One* 7, e41395. <https://doi.org/10.1371/journal.pone.0041395>.

23. Li, H., Yang, C., Lu, K., Zhang, L., Yang, J., Wang, F., Liu, D., Cui, D., Sun, M., Pang, J., et al. (2016). A long-distance fluid transport pathway within fibrous connective tissues in patients with ankle edema. *Clin. Hemorheol. Microcirc.* 63, 411–421. <https://doi.org/10.3233/ch-162057>.
24. Li, H., Yang, C., Yin, Y., Wang, F., Chen, M., Xu, L., Wang, N., Zhang, D., Wang, X., Kong, Y., et al. (2019). An extravascular fluid transport system based on structural framework of fibrous connective tissues in human body. *Cell Prolif.* 52, e12667. <https://doi.org/10.1111/cpr.12667>.
25. Li, H., Lyu, Y., Chen, X., Li, B., Hua, Q., Ji, F., Yin, Y., and Li, H. (2021). Layers of interstitial fluid flow along a "slit-shaped" vascular adventitia. *J. Zhejiang Univ. Sci. B* 22, 647–663. <https://doi.org/10.1631/jzus.B2000590>.
26. Chary, S.R., and Jain, R.K. (1989). Direct measurement of interstitial convection and diffusion of albumin in normal and neoplastic tissues by fluorescence photobleaching. *Proc. Natl. Acad. Sci. USA* 86, 5385–5389. <https://doi.org/10.1073/pnas.86.14.5385>.
27. Dafni, H., Israely, T., Bhujwala, Z.M., Benjamin, L.E., and Neeman, M. (2002). Overexpression of vascular endothelial growth factor 165 drives peritumor interstitial convection and induces lymphatic drain: magnetic resonance imaging, confocal microscopy, and histological tracking of triple-labeled albumin. *Cancer Res.* 62, 6731–6739. <https://doi.org/10.1002/cncr.10960>.
28. Ng, C.P., Hinz, B., and Swartz, M.A. (2005). Interstitial fluid flow induces myofibroblast differentiation and collagen alignment in vitro. *J. Cell Sci.* 118, 4731–4739. <https://doi.org/10.1242/jcs.02605>.
29. Li, H., Yin, Y., Yang, C., Chen, M., Wang, F., Ma, C., Li, H., Kong, Y., Ji, F., and Hu, J. (2020). Active interfacial dynamic transport of fluid in a network of fibrous connective tissues throughout the whole body. *Cell Prolif.* 53, e12760. <https://doi.org/10.1111/cpr.12760>.
30. Kong, Y.Y., Yu, X.B., Huang, R., Li, Z.M., Yin, Y.J., and Li, H.Y. (2021). Preliminary study on the drainage effect of the venous and arterial perivascular and adventitia connective tissue on edema of lower limbs in mice. *Chin. J. Geriatr.* 40, 1057–1061. <https://doi.org/10.3760/cma.j.issn.0254-9026.2021.08.026>.
31. Li, H., Tong, J., Cao, W., Chen, M., Li, H., Dai, H., Xu, L., and Chen, X. (2014). Longitudinal non-vascular transport pathways originating from acupuncture points in extremities visualised in human body. *Chin. Sci. Bull.* 59, 5090–5095. <https://doi.org/10.1007/S11434-014-0633-7>.
32. Adrian, R.J. (1984). Scattering particle characteristics and their effect on pulsed laser measurements of fluid flow: speckle velocimetry vs particle image velocimetry. *Appl. Opt.* 23, 1690–1691. <https://doi.org/10.1364/ao.23.001690>.
33. Keane, R.D., and Adrian, R.J. (1992). Theory of cross-correlation analysis of PIV images. *Appl. Sci. Res.* 49, 191–215. <https://doi.org/10.1007/BF00384623>.
34. Raffel, M., Willert, C.E., and Kompenhans, J. (1998). *Particle Image Velocimetry: A Practical Guide* (Springer).
35. Thielicke, W., and Sonntag, R. (2021). Particle Image Velocimetry for MATLAB: Accuracy and enhanced algorithms in PIVlab. *JORS* 9, 12. <https://doi.org/10.5334/jors.334>.
36. Levick, J.R., and Michel, C.C. (2010). Microvascular fluid exchange and the revised Starling principle. *Cardiovasc. Res.* 87, 198–210. <https://doi.org/10.1093/cvr/cvq062>.
37. Mestre, H., Tithof, J., Du, T., Song, W., Peng, W., Sweeney, A.M., Olveda, G., Thomas, J.H., Nedergaard, M., and Kelley, D.H. (2018). Flow of cerebrospinal fluid is driven by arterial pulsations and is reduced in hypertension. *Nat. Commun.* 9, 4878. <https://doi.org/10.1038/s41467-018-07318-3>.
38. Li, H.Y. (2023). Verification and challenges of interstitial fluid circulatory network. *Chin. J. Front. Med. Sci. (Electr. Vers)* 15, 75–80. <https://doi.org/10.12037/YXQY.2023.08-12>.
39. Kedarasetti, R.T., Drew, P.J., and Costanzo, F. (2020). Arterial pulsations drive oscillatory flow of CSF but not directional pumping. *Sci. Rep.* 10, 10102. <https://doi.org/10.1038/s41598-020-66887-w>.
40. Li, H.Y., Wang, F., Chen, M., Zheng, Z.J., Yin, Y.J., Hu, J., Li, H., Sammer, A., Feigl, G., Maurer, N., et al. (2021). An acupoint-originated human interstitial fluid circulatory network. *Chin. Med. J.* 134, 2365–2369. <https://doi.org/10.1097/cm9.00000000000001796>.
41. Haller, J.T., Wiss, A.L., May, C.C., Jones, G.M., and Smetana, K.S. (2019). Acute management of hypertension following intracerebral hemorrhage. *Crit. Care Nurs. Q.* 42, 129–147. <https://doi.org/10.1097/CNQ.0000000000000247>.
42. Badea, C.T., Guo, X., Clark, D., Johnston, S.M., Marshall, C.D., and Piantadosi, C.A. (2012). Dual-energy micro-CT of the rodent lung. *Am. J. Physiol. Lung Cell. Mol. Physiol.* 302, L1088–L1097. <https://doi.org/10.1152/ajplung.00359.2011>.
43. Li, M., Wang, Z., Xu, Q., Zhang, Z., Cheng, Z., Liu, S., Liu, B., Wei, C., and Wei, L. (2019). A study on noise reduction for dual-energy CT material decomposition with autoencoder. *RDTM* 3, 44. <https://doi.org/10.1007/s41605-019-0122-2>.
44. Zhang, Z., Zhang, X., Hu, J., Xu, Q., Li, M., Wei, C., Wei, L., and Wang, Z. (2021). An optimized K-edge signal extraction method for K-edge decomposition imaging using a photon counting detector. *Front. Phys.* 8, 601623. <https://doi.org/10.3389/fphy.2020.601623>.
45. Li, H.Y., Yang, J.-F., Chen, M., Xu, L., Wang, W.-C., Wang, F., Tong, J.-B., and Wang, C.-Y. (2008). Visualized regional hypodermic migration channels of interstitial fluid in human beings: are these ancient meridians? *J. Altern. Complement. Med.* 14, 621–628. <https://doi.org/10.1089/acm.2007.0606>.
46. Wang, H., and Wang, Z. (2016). Statistical analysis of yarn feature parameters in C/Epoxy plain-weave composite using micro CT with high-resolution lens-coupled detector. *Appl. Compos.* 23, 601–622. <https://doi.org/10.1007/s10443-016-9476-5>.
47. Sasao, J., Tarver, S.D., Kindscher, J.D., Taneyama, C., Benson, K.T., and Goto, H. (2001). In rabbits, landiolol, a new ultra-short-acting  $\beta$ -blocker, exerts a more potent negative chronotropic effect and less effect on blood pressure than esmolol. *Can. J. Anaesth.* 48, 985–989. <https://doi.org/10.1007/BF03016588>.

## STAR★METHODS

## KEY RESOURCES TABLE

REAGENT or RESOURCE	SOURCE	IDENTIFIER
<b>Antibodies</b>		
Anti-CD31 Rabbit pAb	ServiceBio	Cat#GB11063-2; RRID: AB_2922436
<b>Chemicals, peptides, and recombinant proteins</b>		
Gd-DTPA	MedChem Express	Cat#HY-107353
Silver nitrate	Sigma-Aldrich	Cat#7761-88-8
Fluorescein sodium	Sigma-Aldrich	CAS: 518-47-8
Rhodamine B	Sigma-Aldrich	CAS: 81-88-9
Indocyanine green	Sigma-Aldrich	CAS:3599-32-4
Fluorescein isothiocyanate–dextran average mol wt 3000-5000Da	Sigma-Aldrich	Cat#68059
Fluorescein isothiocyanate–dextran average mol wt 70000Da	Sigma-Aldrich	Cat#53471
Cy7	MedChem Express	Cat#HY-D0825
<b>Critical commercial assays</b>		
Hematoxylin and Eosin Staining Kit	BASO	Cat#BA4025
Elastica van Gieson Staining Kit	BASO	Cat#BA4083A
Esmolol Hydrochloride Injection 2 mL:0.2g	QILU PHARMACEUTICAL	111619
<b>Deposited data</b>		
Raw data and statistical analysis	This paper	Mendeley Data: <a href="https://doi.org/10.17632/489myzx57h.1">https://doi.org/10.17632/489myzx57h.1</a>
<b>Software and algorithms</b>		
Origin 2022	OriginLab	<a href="https://www.originlab.com/">https://www.originlab.com/</a>
IBM SPSS Statistics 27	IBM	<a href="https://www.ibm.com/support/pages/downloading-ibm-spss-statistics-27">https://www.ibm.com/support/pages/downloading-ibm-spss-statistics-27</a>
MATLAB R2016a	MathWorks	<a href="https://ww2.mathworks.cn/products/matlab.html">https://ww2.mathworks.cn/products/matlab.html</a>
Zen 3.2	ZEISS	<a href="https://www.zeiss.com.cn/microscopy/products/microscope-software/zen.html#downloads">https://www.zeiss.com.cn/microscopy/products/microscope-software/zen.html#downloads</a>

## RESOURCE AVAILABILITY

## Lead contact

Further information and requests for resources and reagents should be directed to and will be fulfilled by the Lead Contact, Hongyi Li ([leehongyi@bjhmoh.cn](mailto:leehongyi@bjhmoh.cn)).

## Materials availability

This study did not generate new unique reagents.

## Data and code availability

- Raw data and statistical analysis in this paper have been deposited at Mendeley Data, and are publicly available as of the date of publication. DOIs are listed in the [key resources table](#). Imaging data reported in this paper will be shared by the [lead contact](#) upon request.
- This paper does not report original code.
- Any additional information required to reanalyze the data reported in this paper is available from the [lead contact](#) upon request.

## EXPERIMENTAL MODEL AND STUDY PARTICIPANT DETAILS

### Animals

All animal experiments were approved by the Institutional Animal Care and Use Committee of the Institute of Basic Medical Sciences Chinese Academy of Medical Sciences, Peking Union Medical College (No. ACUC-A02-2021-017) and performed according to institutional guidelines and research protocols approved by the Institutional Animal Care and Use Committee of the Institute of Basic Medical Sciences Chinese Academy of Medical Sciences, Peking Union Medical College. A total of 96 male and 96 female Sprague–Dawley rats, 20–25 weeks old, 300–350g in weight (HFK Bio-Technology, Beijing, China), were used and housed in pathogen-free conditions with 12 h of continuous light and 12 h of continuous darkness at the Laboratory Animal Center of the Institute of Basic Medical Sciences Chinese Academy of Medical Sciences. Equal numbers of male and female rats were taken to ensure that sex of the animals does not constitute a biological variable during analysis. The procedures designed minimize animal suffering and respect the 3Rs principles. The rats were anesthetized with isoflurane (1%) in 1 L/min oxygen or intraperitoneally anesthetized (pentobarbital 50 mg/kg) during experiments. Body temperature was maintained at 37.5°C with a rectal probe-controlled heated platform. A ventilator (RoVent Jr., Kent Scientific, USA; V100, YUYAN, China) was used to regulate the frequency, TV, and I/E (inhalation/exhalation) of breath. The rats were euthanized by carbon dioxide according to the guidelines of the American Veterinary Medical Association (AVMA).

## METHOD DETAILS

### The selection of the imaging tracers

Using fluorescent stereomicroscopy (Axio Zoom.V16, Zeiss) and the spectral micro-computed tomography (SMCT),<sup>42–44</sup> we examined which tracers were able to flow in the adventitial pathways along the vessels of the lower limbs in rats, including several large (>1 kDa) and small (<1 kDa) molecular weight, water- and lipid-soluble tracers (Table S4). It was found that the fluorescein sodium (FluoNa) can be used for *in vivo* real-time fluorescent imaging with a higher spatial resolution than Rhodamine B and Indocyanine green, and the silver nitrate can be used for *in situ* imaging within tissues and organs (Figure 1, Video S12). The gadolinium-diethylenetriamine pentaacetic acid (Gd-DTPA) was used in MRI experiments. The FITC-dextran (70,000 dalton) was used to visualize the lymphatic vessels accompanying the femoral vessels.

### Adventitial infusion and intravenous injection

For intravenous injection, the selected tracer was injected into the saphenous vein at the level of right knee. For adventitial infusion by fluorescent tracer, 4 $\mu$ L solution of FluoNa (diluted to 0.1 g/L in normal saline (NS)) was dripped onto the adventitia on the saphenous or femoral arteries or veins of the lower limbs, axillary artery and vein of the upper limbs or the left common carotid artery in the middle neck or the anterior descending arteries near the apex of the heart using the tip of the 10  $\mu$ L pipette. 40 $\mu$ L FluoNa (0.01 g/L in NS) was used for intravenous injection.

Consistent with the imaging methods in our previous studies,<sup>22,25,45</sup> the adventitial infusion for MRI or SMCT was the hypodermic injection of the Gd-DTPA or silver tracer into the right or left ankle dermis. This method is equivalent to injecting the tracer into the perivascular tissues of the accompanying saphenous artery and vein under ankle dermis. The duration for the hypodermic injection into ankle dermis was 5–10s. 200  $\mu$ L Gd-DTPA (0.5 mmol/mL in NS, MedChem Express, Quality Research, Zhuozhou, Hebei, China) was used for adventitial infusion or intravenous injection, respectively. 400 $\mu$ L silver nitrate solution (10% in deionized water) was injected into ankle dermis for the cardiac perfusion by adventitial infusion and 1 mL silver nitrate (2% in deionized water) for intravenous injection. 4 $\mu$ L silver nitrate solution (10% in deionized water) was dripped onto the adventitia on the saphenous arteries and veins in the lower limbs to detect whereabouts the adventitial ISF flowed along the saphenous vessels. The angiography was performed by injecting the tracer into the tail vein.

### Image acquisition by MRI

5 rats were used for adventitial infusion and 3 rats for intravenous injection via tail vein. Imaging was performed by 9.4T MRI scanner (Biospec 94/30 USR Bruker, Ettlingen, Germany) with a rat body volume coil. A respiratory sensor (SA Instruments, Stony Brook, NY, USA) was placed under the abdomen to monitor the respiration rate. Scanning parameters were adjusted to obtain a high spatial resolution. The coronal images were collected with a 3D FLASH sequence: TR = 11 ms, TE = 1.84 ms, flip angle = 10°, FOV = 90  $\times$  31  $\times$  23 mm, matrix size = 510  $\times$  176  $\times$  131, resolution = 176  $\mu$ m isotropic, number of averages = 1, acquisition time was 5 min. Immediately after the administration of the Gd-DTPA, each rat was dynamically scanned for a total of 50 min. The raw data were analyzed at a Dell Precision Tower workstation (T7910) with multi-planar reconstruction (MPR) and maximum-intensity projection (MIP) reconstructions.

### *In vivo* fluo-imaging of adventitial pathways in limb

After the skin along the vessels of the limbs opened surgically in 6 rats, the FluoNa was administrated by adventitial infusion on the saphenous vessels or intravenous injection into the saphenous vein, respectively. The real-time flow of the fluorescent adventitial ISF along the arterial and venous vessels in the limbs (Figures 1B and 1G) was recorded by the fluorescence stereomicroscope with a high-sensitivity camera (Prime BSI Scientific CMOS, Teledyne, USA). After recording, sections of the stained arteries and veins at the distal and proximal injection site (Figures 1C, 1D, 1H, and 1I) were sampled for the real-time frozen fluorescence and histological analysis.

In another 5 rats, a 3–5 mm segment of the right or left femoral vessels was isolated and exposed to air by surgically stripping their perivascular tissues (Figures 2A, 2B, 2C, S3A, and S3A1) while the intravascular blood flow was kept intact. The continuous flow of the adventitial

FluoNa along the isolated femoral artery and vein was clearly recorded when the FluoNa was administrated onto the adventitia of the distal saphenous vessels. After recording, the distal femoral vessels stripped of perivascular tissues (Figures 2M, 2M1, 2O, 2O1, S3B–S3D1) and the proximal femoral vessels with perivascular tissues (Figures 2H, 2H1, 2J, 2J1, S2B, and S2B1) of the same rat were sampled for the real-time frozen fluorescence and histological analysis, respectively.

After the adventitia along the isolated femoral vein and artery was bathed by 10 $\mu$ L solution of type I collagenase (0.1 g/mL in NS, Sigma-Aldrich) for 30 min in the other 6 rats, it was observed whether the distal FluoNa could pass through these disrupted adventitial pathways (Figures 2D, S2C, and S2C1). By intravenous injection of the FluoNa into the lumen of the distal saphenous vein (2/6 rats) or the contralateral saphenous vein (2/6 rats), it was observed whether the blood flow of these femoral vessels was unobstructed (Figure 2E). In the last 2/6 rats with the disrupted adventitia, the femoral vessels were sampled for the frozen fluorescence analysis after the adventitial infusion of the FluoNa (Figures S2C and S2C1).

In the control group of 3 rats by adventitia-infused NS, the corresponding tissues in the limbs, abdomen and thorax were sampled for frozen fluorescence or histological analysis. To visualize the lymphatics, 200 $\mu$ L solution of FITC-dextran (1%, 70 kDa, Sigma-Aldrich) was injected hypodermically into the ankle dermis of 3 rats. At 10 min after the administration, the lymphatic besides the femoral artery and vein was clearly visualized under fluorescence stereomicroscope (Figures S3K–S3K2). The corresponding tissues in the limbs were sampled for frozen fluorescence and histological analysis.

### Measuring rapid and speckle-like flow rate

Limited by the spatial and temporal resolution of MRI, we investigated the flow rate of adventitial ISF using fluorescein. Immediately after the FluoNa administration by real-time fluorescence stereomicroscope with high-sensitivity camera, the early and subsequent flow of the fluorescent adventitial ISF was recorded dynamically along the femoral vessels with stripped perivascular tissues. The distance between the administration site and the observation point, and the early time of fluorescein appearance on the femoral vessels were recorded in 3 rats. The speckle-like flow along the femoral veins was recorded in a total of 24 rats (Table S2).

We developed a method of STV to measure the continuous FluoNa flow by speckle pattern translation recording, which has been extensively used in measuring displacements and velocities.<sup>32,34,35</sup> The STV consists mainly of two steps: 1) Pre-processing; 2) Velocimetry. 1) By analyzing the data of the fluorescent adventitial ISF flow, we found several difficulties in measuring velocities in the videos, such as the low-frequency background light flickering and the quiver of the vessel itself. Therefore, in the first step, we designed an algorithm to overcome these difficulties based on some image processing methods, such as high-pass filter, image registration, and mean-image subtraction. 2) For the velocimetry, the region of interest was divided into small patches (as the rectangle in Figure S5A). Afterward, for each small patch, cross-correlation<sup>33</sup> was performed to estimate the most probable displacement within its surrounding area in the next frame. Then, displacement per time between adjacent frames yielded the velocity for each patch (as the vector field in Figure S5A). The velocity field of the continuous adventitial ISF flow along the femoral vein was analyzed by the STV in 3 live rats (Figures S5B and S5C). The real-time flow of adventitial ISF along the femoral veins was recorded by the fluorescence stereomicroscopy while recording synchronized measurements of the electrocardiogram (ECG) and the respiratory cycle by animal physiological monitoring device (PowerLab, AD Instruments, Australia). The speed change curves were found to match the changes of heartbeats and respiration.

The flow rate changes of the FluoNa along the femoral veins under physiological and non-physiological conditions were further investigated by STV. The changes of the adventitial ISF flow velocity at different heart rate (HR) were recorded in a typical rat (Figure 3B). The HR was lowered by tail vein injection of Esmolol (2.0–3.0 mg/kg/min). The effects of the different respiratory parameters on the adventitial ISF flow were investigated in 6 live (Figures 3D1, 3F1, and 3H1) and 6 freshly dead rats (Figures 3E1, 3G1, 3I1), such as respiratory rate (RR), inspiratory expiratory ratio (I/E) and tidal volume (TV). The freshly dead rats referred to the rats that were euthanized by carbon dioxide and used for the experiments within 1 h after the heartbeat and breathing completely stopped for 15 min (detected by ECG and respiration signal monitoring of PowerLab). Two pressure-measuring guidewires were placed in the contralateral iliac vein and artery of each rat. The systolic and diastolic arterial pressures, venous pressures of iliac vessels were measured under different respiratory parameters (RR: 30-60-90bpm, I/E: 1:1-1:2-2:1, TV: 4.0-6.0-8.0 mL), respectively. The changes of the arterial and venous pressures were recorded by PowerLab. The changes of breathing (Resp.) were the measured pressure on the surface of the body of the rats by the breathing band sensor.

### Qualitative observation on circulatory pathways

To depict the circulatory pathways of adventitial ISF along the systemic vasculature, we tracked the longitudinal flow of adventitial ISF along several major systemic arteries and veins by the adventitial infusion of the FluoNa onto the right saphenous vessels, axillary vessels, and the left carotid artery of the neck in 9 rats, respectively (Figure S7A). The distal and proximal ends of the vessels around the injection site were sampled for the real-time fluorescence stereomicroscopy or histological analysis. The fluorescently stained right anterior vena cava (AVC), inferior vena cava (IVC), and aorta were sampled and compared with those of adventitial infusion by NS.

To delineate the cycle of adventitial ISF flow along the pulmonary vasculature, the pulmonary artery, vein, and the surrounding tissues between the artery and vein at the level of the right middle lobe of lungs were sampled at 50s, 2 min, 3 min after the adventitial infusion of the FluoNa into the right ankle dermis in 9 rats, respectively. In other 4 rats, the FluoNa was administrated on the surface of the root of the pulmonary artery or a segment of the pulmonary vein in the middle lobe of right lung, respectively. At 10s after the administration, the movement of the FluoNa was recorded by fluorescence stereomicroscopy.

To disclose the flow direction of adventitial ISF along the coronary arteries of a beating heart, the FluoNa was dropped into the superficial tissues on the ventricular apex of 3 rats, and dynamically recorded with a high-speed camera for 5 min.

### Ex vivo fluo-imaging and histological analysis

Frozen fluorescent section slices (4  $\mu\text{m}$  thickness) were obtained using calibrated vibratome (VT1200S, Leica). One section was selected every 5 sections for each sample of the arterial and venous vessels, heart, or lungs. All slices were imaged by the fluorescence microscope (Scope.A1, Zeiss, German) with a digital camera (Axiocam 506, Zeiss, German). Exposure time, magnification, and luminous intensity under a dark environment were kept the same for all groups. Quantification of fluorescence intensity of the slices was performed by ImageJ (1.8.0). In the cross-sectional images of the vascular vessels of each rat, the arterial, venous walls, and perivascular tissues were equally divided into 5 regions. The maximum fluorescence intensity value in each region was recorded. There were 3 rats in each experimental or control group. Thus, a total of 15 fluorescence intensity value of the arterial, venous walls, and the surrounding tissues were obtained for each group. The same thresholds were used for the slices of each group. The frozen slices were also studied by Elastica van Gieson staining. The hematoxylin and eosin (H&E) staining and the immunostaining of the antibodies against CD31 (Servicebio, Wuhan, China) were performed according to routine procedures.

### Effects of heartbeat or breath on adventitial flow

Under physiological conditions, it was found that the adventitial ISF flow was continuous centripetally along the femoral vessels and fluctuated with respiration motions at high tidal volumes. To investigate the effects of each heartbeat or breath on the adventitial ISF flow, we performed the following experiments by means of chest compressions, open-chest atrial or ventricular compressions, and mechanical ventilation in freshly dead rats, respectively. The flow rate of the adventitial ISF flow along the femoral veins was measured by the STV as well. The systolic and diastolic arterial pressures, venous pressures of iliac vessels were measured under the respiratory parameters (RR: 90bpm, I/E: 1:1, TV: 6.0 mL). When cardiac and respiratory arrest, all dead rats were given heparin (125 IU/kg) for anticoagulation via the tail vein before the following experiments.

By chest compressions at a frequency of about 30 per minute, the flow rate of adventitial ISF was recorded in 3 freshly dead rats (Figure 4A). The duration of one-shot compression was around 1s. By surgically opening the chest cavity, the effects of each contraction and dilation of atria or ventricles on the adventitial ISF flow were observed when the atria or ventricles were directly compressed in 6 rats, respectively (Figures 4B and 4C). The compressions of the atria or ventricle were performed by a digital force gauge (HF-10, HighTec, China) at the force around 0.5 N. The duration of one-shot compression was around 10s. The free relaxation time of the atrium or ventricle after one-shot compression were about 10–15 s. The ECG signals were detected when the heart, atria or ventricles of dead rats were compressed, representing the compressions.

In another 3 freshly dead rats, the effects of each inflation and deflation of the lungs on the adventitial ISF flow were recorded when the lungs were ventilated by a 10 mL syringe (Figure 4D). The inflation and deflation volumes were both 6 mL. The duration of inflation time was around 10 s, and the deflation time was about 10–15 s.

### Cardiac compression or ventilation on ISF flow

The effects on the adventitial ISF flow by the pulsating blood flow and the mechanical pulsations of the vessel walls were studied in 16 freshly dead rats who were given heparin (125 IU/kg) for anticoagulation via the tail vein before sacrifice as well. After preparation, the apex of the heart was surgically removed in all dead rats to expose the left and right ventricular chambers to the air, and the heart was repeatedly compressed to drain the residual blood in the vascular vessels until no more blood was flowed out from the opened chambers. Subsequently, the mechanical motions of the femoral vessel walls were detected by a laser vibrometer (OFV-5000, Polytec). The systolic and diastolic arterial pressures, venous pressures were also measured under certain respiratory parameters (RR 90bpm, I/E 1:1, TV 6.0 mL). Two pressure-measuring guidewires were inserted from the open left ventricular chamber into the abdominal aorta and from the open right ventricular chamber into the abdominal inferior vena cava, respectively. The changes of the arterial and venous pressures were recorded by PowerLab. The adventitia of the right femoral vessels was disrupted by collagenase I (10  $\mu\text{L}$ , 0.1 g/mL in NS) and the left femoral vessels were bathed in NS solution. The flow of the adventitial ISF along the right or left saphenous or femoral veins was recorded dynamically by fluorescence stereomicroscopy and the velocity was measured by STV.

After administration of the FluoNa at the distal end of the adventitial pathways along the left and right saphenous vessels, the heart was pressed at 30–60bpm for 30 min in 6 rats while the lungs were not ventilated (Figure 5C). After administration of the FluoNa at the proximal end of the adventitial pathways along the femoral vessels, the lungs were ventilated for 30 min in another 6 rats while the heart was not compressed (Figure 5H). The results of the adventitial ISF flow along the right and left femoral and saphenous vessels were recorded by fluorescence stereomicroscopy, respectively.

To clarify whether the forces generated by the repeatedly ventilated lungs drive the adventitial ISF flow through the conduction of the pulmonary artery or veins, we continued to use vascular clamps to clamp the root of the main pulmonary artery or the thoracic segment of the inferior vena cava in the last 4 rats, respectively. The real-time flow of FluoNa along femoral vein was observed dynamically under fluorescence stereomicroscopy.

### Distributions of silver nitrate in tissues by SMCT

To determine whereabouts the adventitial ISF flowed along the saphenous vessels or entered the heart, we investigated the adventitial pathways in the lower limb and the cardiac perfusion by adventitial infusion or intravenous injection of the silver nitrate, respectively. 3 rats were used to detect the locations of the adventitial infusion of 4  $\mu$ L silver nitrate solution that was dripped onto the adventitia on the saphenous arteries and veins. The cardiac perfusion by adventitial infusion of silver nitrate was used in 5 rats and the intravenous injection in another 5 rats. If the rats died during the injection, the repeated chest compressions (400 bpm) were given immediately to ensure the circulate of the silver nitrate in the blood to reach 3 min. The rats were sacrificed at 3 min after the administration. The samples of the proximal femoral artery and vein (2 cm from the infusion site), the heart and lungs were sampled. All samples were treated with alcohol gradient dehydration (30%, 50%, 75%, 90%, 100%) before SMCT scanning.

The samples were imaged using a photon counting detector (PCD) based spectral micro-CT scanner (The Institute of High Energy Physics, Chinese Academy of Sciences, China). The PCD (XCounter, Sweden) uses a CdTe crystal with a thickness of 0.75 mm as the sensor material. The detector contains 2,048  $\times$  512 pixels with a pixel size of 100  $\mu$ m. It has two energy thresholds and can detect photons with energy range from 10 keV to 160 keV. By setting the thresholds, two energy window data can be obtained in one CT scan.<sup>42–44</sup>

### Adventitial matrix of femoral vessels by micro-CT

The femoral vessels of 3 rats were sampled and treated with alcohol gradient dehydration (30%, 50%, 75%, 90%, 100%) before micro-CT scanning. High-resolution 3D X-ray micro-CT (nanoVoxel-3000 series; Sanying Precision Instruments Co., Ltd.) was used to get 1800 pics grayscale images of each sample.<sup>24,46</sup> The images were captured on a detector 2940  $\times$  2304 pixels, with an exposure time of 0.45s, a voltage of 60.0 kV, a current of 50  $\mu$ A and a voxel size of 0.85  $\mu$ m. The software VOXEL RECON (Sanying Precision Instruments Co., Ltd.) was adopted to reconstruct algorithm and correct image data.

The numbers of the adventitial fibers between the fascia and the tunica media of the femoral arteries and veins were estimated in the reconstructed 3D images of micro-CT. The area of the adventitial fibers and its surrounding fascia along the femoral artery and vein were identified and extracted. The minimum intensity value of the fibers between the fascia and tunica media was set for connected component analysis. The diameter of the fibers was set to give the cross-sectional area of a fiber. The area of the connected components was then divided by the area of the fibers to obtain the numbers of fibers in the connected components. Then, the numbers of bundles in all slices were counted. The maximum, median and minimum values of fibers in adventitial pathways along both femoral artery and vein were calculated respectively.

### Esmolol experiments in myocardium analysis

The changes of the HR by adventitial infusion or intravenous injection of Esmolol was recorded in 10 alive rats, respectively. The dosage of Esmolol for adventitial infusion or intravenous injection was 0.5 mg/kg and adjusted according to each rat weight.<sup>47</sup> After the adventitial infusion or intravenous injection of Esmolol, another 50 rats were sacrificed at 1, 3, 5, 8, 35 min, respectively. The concentration of Esmolol in ventricular muscles was detected by LC-MS/MS. The samples were homogenized by the grinder (Tiangen-Osey50) with 1  $\mu$ L/mg of methanol acetonitrile (50:50) % (v/v), centrifuged at 4000 rpm (Eppendorf 5810R) for 20 min, and the supernatant was taken for detection. Measurements of the Esmolol were accomplished on a Shimadzu LC-2-AD XR equipped with a binary pump, a degasser, an auto sampler/injector and a column heater (Shimadzu, Kyoto, Japan), coupled to an AB SCIEX QTrap 5500 Mass Spectrometer equipped with an ESI ionization source (AB SCIEX, USA).

### QUANTIFICATION AND STATISTICAL ANALYSIS

Statistical analyses were performed using Origin 2022 software. Paired samples t-test was used to compare the fluorescence intensity of two different points in a single group and two-tailed Student's t-test was used between two groups. The exact p values were calculated at a 0.05 level of significance. All statistical details of experiments can be found in the figure legends including the statistical tests used, exact value of n, what n represents, definition of center, and dispersion and precision measures.